Journal of Medicinal Chemistry

Drug Annotation

4-Methyl-6,7-dihydro-4H-triazolo[4,5-c]pyridine-based P2X7 Receptor Antagonists: Optimization of Pharmacokinetic Properties Leading to the Identification of a Clinical Candidate

Michael A Letavic, Brad M Savall, Brett D. Allison, Leah Aliusio, José-Ignacio Andrés, Meri De Angelis, Hong Ao, Derek A. Beauchamp, Pascal Bonaventure, Stewart Bryant, Nicholas I. Carruthers, Marc Ceusters, Kevin J Coe, Curt A. Dvorak, Ian Fraser, Christine F Gelin, Tatiana Koudriakova, Jimmy Liang, Brian Lord, Timothy W Lovenberg, Monica Otieno, Freddy Schoetens, Devin Maun Swanson, Qi Wang, Alan D Wickenden, and Anindya Bhattacharya

J. Med. Chem., **Just Accepted Manuscript** • Publication Date (Web): 11 May 2017

4-Methyl-6,7-dihydro-4*H*-triazolo[4,5-c]pyridine-based P2X7 Receptor Antagonists: Optimization of Pharmacokinetic Properties Leading to the Identification of a Clinical Candidate

Michael A. Letavic,[1,] Brad M. Savall,[1] Brett B. Allison,[1] Leah Aluisio,[1] Jose Ignacio Andres,[2] Meri De Angelis,[2] Hong Ao,[1] Derek A. Beauchamp,[3] Pascal Bonaventure,[1] Stewart Bryant,[3] Nicholas I. Carruthers,[1] Marc Ceusters,[4] Kevin J. Coe,[1] Curt A. Dvorak,[1] Ian Fraser,[1] Christine F. Gelin,[1] Tatiana Koudriakova,[1] Jimmy Liang,[1] Brian Lord,[1] Timothy W. Lovenberg,[1] Monicah Otieno,[3] Freddy Schoetens,[1] Devin Swanson,[1] Qi Wang,[1] Alan D. Wickenden,[1] and Anindya Bhattacharya[1]*

[1]Janssen Research & Development, LLC, 3210 Merryfield Row, San Diego, California 92121

[2]Janssen Research & Development, A Division of Janssen-Cilag, Jarama 75, 45007 Toledo, Spain

[3]Janssen Research & Development, LLC, 1400 McKean Road, Spring House, PA 19477, United States

[4]Janssen Research & Development, Janssen Pharmaceutica NV, Turnhoutseweg 30, 2340 Beerse, Belgium

KEYWORDS: P2X7, IL-1β, depression, inflammation, JNJ-54175446.

ABSTRACT: The synthesis and pre-clinical characterization of novel 4-(*R*)-methyl-6,7-dihydro-4*H*-triazolo[4,5-c]pyridines that are potent and selective brain penetrant P2X7 antagonists is described. Optimization efforts based on previously disclosed unsubstituted 6,7-dihydro-4*H*-triazolo[4,5-c]pyridines, methyl substituted 5,6,7,8-tetrahydro-[1,2,4]triazolo[4,3-a]pyrazines and several other series lead to the identification of a series of 4-(*R*)-methyl-6,7-dihydro-4*H*-triazolo[4,5-c]pyridines that are selective P2X7 antagonists with potency at the rodent and human P2X7 ion channels. These novel P2X7 antagonists have suitable physicochemical properties and several analogs have an excellent pharmacokinetic profile, good partitioning into the CNS and show robust in vivo target engagement after oral dosing. Improvements in metabolic stability led to the identification of JNJ-54175446 (**14**) as a candidate for clinical development. The drug discovery efforts and strategies that resulted in the identification of the clinical candidate are described herein.

INTRODUCTION

Depression is a debilitating disease that afflicts millions of adults at some time during their life, and chronic depression can shorten lifespan by over ten years.[1] Many patients do not respond to current antidepressant treatments, or become resistant to current medications, and as a result there have been significant efforts to uncover novel mechanisms to treat depression. Unfortunately, identifying compounds targeting novel mechanisms with clinical utility for the treatment of mood disorders has been a daunting task. Recent studies suggest that there may be a link between neuro-inflammation and mood disorders[2] and there is an emerging body of work that implicates the production of proinflammatory cytokine IL-1β as a key mediator of neuro-

inflammation.[3] Interestingly, the P2X7 ion channel is expressed abundantly in microglia in the CNS where it is involved in IL-1β release.[4,5] and microglial IL-1β appears to be a significant source of CNS IL-1β. Inhibition of P2X7 and P2X7 mediated IL-1β release might therefore represent a novel approach to the treatment of mood disorders. Indeed, there have been several reports suggesting a role for P2X7 in pre-clinical models of mood disorders[6] and very recently two groups reported on the efficacy of P2X7 antagonists in chronic models of depression.[7] However, to our knowledge, the effect of a P2X7 antagonist on depression or any related mood disorder has not yet been tested in the clinic.

Several companies have progressed P2X7 antagonists into clinical development and tested the P2X7 mechanism for peripheral indications including rheumatoid arthritis (RA), Crohn's disease and osteoarthritic pain. Some examples of compounds that entered clinical trials are depicted in Chart 1. The AstraZeneca compound, AZD9056 (**1**)[8] has been tested in both RA and Crohn's disease.[9] The compound proved ineffective at treating RA, but achieved the primary clinical efficacy endpoint in a small proof-of-concept study in Crohn's disease. Pfizer reported Phase IIb results for their lead compound (**2**, CE-224,535)[10] and in a three month trial in RA patients **2** was shown to inhibit the release of IL-1β in blood but did not show efficacy in RA.[11] Both of these compounds are peripherally restricted, and therefore would likely not be useful for treating CNS disorders. Notably, **1** demonstrated improvements in mental component score (SF-36) in the Crohn's study. GlaxoSmithKline progressed the pyroglutamate-based compound (**3**, GSK1482160) into clinical development, but never moved beyond Phase I studies, possibly due to a lack of safety margins.[12] This compound is reported to be a negative allosteric modulator of P2X7 and has good CNS penetration (brain/blood ratio of ~0.5).[13]

Chart 1. Select P2X7 Antagonist Clinical Candidates.

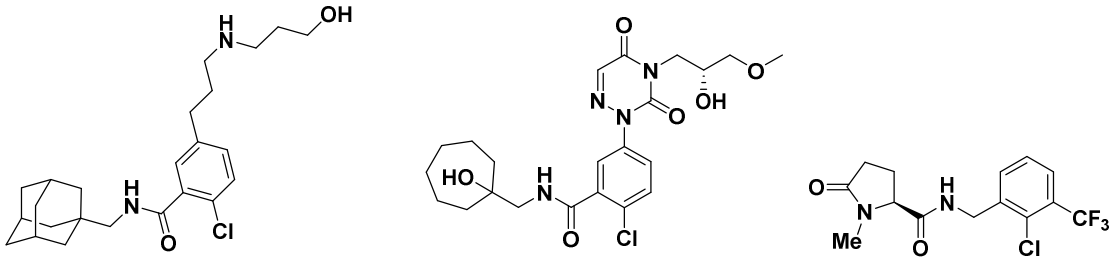

The first CNS penetrant compounds disclosed by Janssen are compounds **4** and **5** on Chart 2. These compounds are potent human and rat P2X7 antagonists that efficiently penetrate the CNS[14] and they have proven to be good tool compounds for pre-clinical efficacy studies. In fact, **4** was shown to inhibit the stimulated release of IL-1β in rat brain, and to attenuate amphetamine induced hyperactivity in rat.[15] Compound **4** has also shown effects in models of schizophrenia,[16] temporal lobe epilepsy[17] and in seizure models[18] and compound **5** increased social interactions in a model of social stress.[19] Unfortunately, this class of compounds suffers from poor pharmacokinetic properties and we were unable to progress any of these analogs into clinical development. Due to the very interesting CNS effects that were observed with compounds **4** and **5**, we sought to identify novel, CNS penetrant compounds with pharmacokinetic profiles consistent with once daily oral dosing in human.

Following the disclosure of a series of 5,6,7,8-tetrahydro-[1,2,4]triazolo[4,3-a]pyrazines[20] by GSK that are potent P2X7 antagonists we decided to investigate the effects of substitution on the

tetrahydropyrazine core and this led to the identification of the 8-methyl-5,6,7,8-tetrahydro-[1,2,4]triazolo[4,3-a]pyrazines as exemplified by **6** on Chart 3.[21]

Chart 2. CNS Penetrant Lead P2X7 Antagonists.

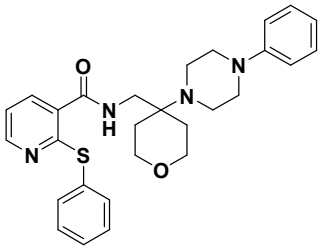

4, JNJ-47965567
***h*pIC$_{50}$=8.3**
***r*pIC$_{50}$=7.8**

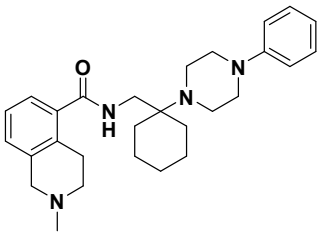

5, JNJ-42253432
***h*pIC$_{50}$=7.7**
***r*pIC$_{50}$=7.8**

These, and related structures, also demonstrated that substitution on the core ring could have dramatic effects on potency, speciation, and DMPK properties. At the same time a number of additional cores were also discovered including the 6,7-dihydro-4*H*-triazolo[4,5-c]pyridines (e.g., **7**),[22] 4,5,6,7-tetrahydro-1*H*-imidazo[4,5-c]pyridines (e.g., **8**),[23] and 6,7-dihydro-[1,2,4]triazolo[4,3-a]pyrazin-8(5*H*)-ones (e.g., **9**),[24] among others.[25]

Chart 3. Optimized CNS Active Lead Compounds.

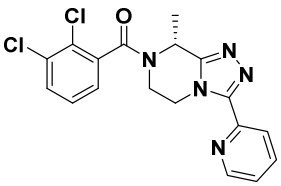

6
***h*P2X7 IC$_{50}$ = 1.4 nM**
***r*P2X7 IC$_{50}$ = 760 nM**

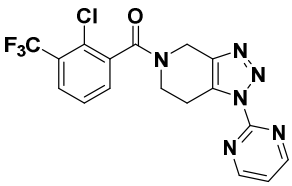

7
***h*P2X7 IC$_{50}$ = 4 nM**
***r*P2X7 IC$_{50}$ = 7 nM**

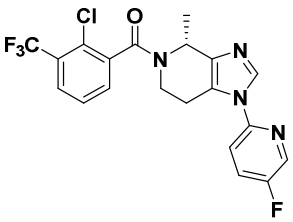

8, JNJ-54166060
***h*P2X7 IC$_{50}$ = 4.0 nM**
***r*P2X7 IC$_{50}$ = 115 nM**

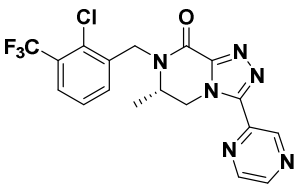

9
***h*P2X7 IC$_{50}$ = 0.7 nM**
***r*P2X7 IC$_{50}$ = 79 nM**

This publication details the results of efforts to optimize the in vivo properties of analogs prepared from the 4-methyl-6,7-dihydro-4*H*-triazolo[4,5-c]pyridine core, some challenges that were encountered and the solutions that were found which resulted in the identification of a clinical candidate with the potential to be useful for the treatment of mood disorders.

RESULTS AND DISCUSSION

Previous publications highlighting compounds **6-9** established much of the in vitro SAR for the 6,5 fused heterocyclic-based structures. This work confirmed that the 2-chloro-3-trifluromethyl benzamide, or similar 2,3-di-substituted benzamides, were the preferred substituents on the piperidine (or piperazine) nitrogen for P2X7 potency and also demonstrated the benefit of placing a substituent, such as methyl, on the tetrahydropyridine ring which resulted in both improvements in potency, and reduced speciation. In many cases the methyl substituent also improved metabolic stability in microsomal preparations. These efforts also established that a heteroaromatic substituent was preferred at the *N*-1 position of the 1,2,3 triazole, imidazole or *C*-3 position of the 1,2,4 triazole. In order to assess the effect of the *N*-1 substituent on in vivo properties of the 4-(*R*)-methyl-6,7-dihydro-4*H*-triazolo[4,5-c]pyridines a limited set of new analogs were synthesized (Table 1). The heteroaromatics that were installed on compounds **10-14** were chosen based on previous SAR with respect to potency, metabolic stability and CYP inhibition profiles. The in vitro data for these compounds are shown on Table 1. All five compounds have acceptable molecular weights and similar cLog P's and P2X7 potencies. As was noted in an earlier publication,[21] installation of the methyl group on the core ring of related structures sometimes improved rat P2X7 potency rather dramatically[22] and in this set, this was also true for compounds **11** and **13**. Next, these new compounds were comprehensively profiled in vitro and in vivo.

Table 1. SAR for Select 4-(*R*)-methyl-6,7-dihydro-4*H*-triazolo[4,5-c]pyridines.

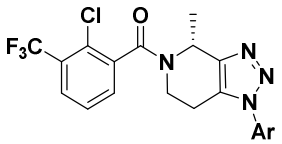

10-14

Compd	Ar	MW	cLog P	*h*P2X7 pIC_{50} [a]	*r*P2X7 pIC_{50} [b]
10	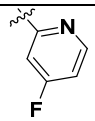	439.8	3.90	8.08±0.08	7.91±0.06
11		422.8	2.82	8.46±0.25	8.04±0.34
12		422.8	2.82	8.66±0.29	8.69±0.27
13	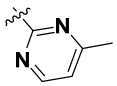	436.8	3.30	8.27±0.25	8.18±0.15
14	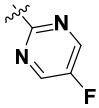	440.8	3.00	8.46±0.36	8.81±0.24

[a] human FLIPR pIC_{50} measured in a Ca^{2+} flux assay, [b]rat FLIPR pIC_{50} measured in a Ca^{2+} flux assay, all data are the result of at least three assays run in triplicate with the mean value reported; $pIC_{50} \pm$ s.d. is reported.

Tables 2 and 3 contain data for microsomal stability, hERG binding, protein binding and solubility for compounds **10-14**. To summarize, none of the compounds had significant hERG binding, all had acceptable protein binding and solubility varied from acceptable to very good. Microsomal stability varies significantly for this set of compounds with human extraction ratios ranging from 0.66 to <0.30. The first compound that was prepared was compound **11** and this compound was the first to be profiled in vivo. Prior to this, compound **11** was screened against a panel of 50 ion channels, receptors and transporters (Eurofins-CEREP,

http://www.eurofins.com/) and a general kinase panel and did not have any significant activity (tested at 1 μM) in any of the assays.

Table 2. Microsomal Stability Data and hERG IC_{50}'s for Compounds **10-14**.

Compd	RLM Stability[a]	HLM Stability[b]	MLM Stability[c]	DLM Stability[d]	CMLM Stability[e]	hERG IC_{50}[f]
10	0.48	0.54	n.t.	n.t.	n.t.	>10
11	0.68	0.66	0.50	0.57	0.85	>10
12	0.33	0.39	0.40	<0.26	0.85	>10
13	0.78	0.36	0.29	0.29	0.91	>10
14	<0.2	<0.3	<0.25	<0.26	<0.19	>10

[a]Stability in rat liver microsomes. [b]Stability in human liver microsomes. [c]Stability in mouse liver microsomes. [d]Stability in dog liver microsomes. [e]Stability in cynomolgus monkey liver microsomes. All data are reported as hepatic extraction ratios where the predicted hepatic clearance is divided by the species specific hepatic blood flow. [f]hERG IC_{50} in μM as measured in an [^{3}H]-dofetilide competition binding assay in HEK-293 cells expressing the hERG channel.

Table 3. Select In Vitro Data for Compounds **10-14**.

Compd	Rat PPB[a]	Human PPB[a]	Mouse PPB[a]	Rat brain binding[b]	Solubility @ pH 2	Solubility @ pH 7
10	94.8%	97.6%	95.8%	n.t.	4.8 μM	2.1 μM
11	93.7%	91.6%	94.7%	95.0%	48.2 μM	94.4 μM
12	92.4%	91.6%	92.6%	n.t.	>400 μM	180 μM
13	90.5%	91.5%	90.5%	95.9%	328 μM	283 μM
14	87.8%	88.8%	88.7%	94.9%	38.7 μM	20.7 μM

[a]Preliminary (Tier 1) data. [b]Rat brain tissue binding.

Compound **11** was dosed in rat and dog and the pharmacokinetic profiles are summarized in Table 4. Compound **11** has relatively high clearance in both species, consistent with the microsomal data shown on Table 2.

Table 4. Rat and Dog Pharmacokinetic Parameters for Compound **11**.

Species	CL (mL/min/kg)[a]	V_{ss}(L/kg)[b]	$t_{1/2}$ (h)[c]	%F
Rat[d]	46	3.0	1.5	77%
Dog[e]	33	3.3	2.4	65%

[a]Clearance, [b]volume of distribution at steady state, [c]i.v.half-life. [d]dosed at 1 mg/kg i.v. and 5 mg/kg p.o. [e]dosed at 1 mg/kg i.v. and 3 mg/kg p.o.

In order to further assess the in vivo properties of compound **11** two studies were performed. First, P2X7 target engagement was assessed in rat using ex-vivo autoradiography. Data are shown in Figure 1. Compound **11** dose dependently occupied the P2X7 ion channel with an ED_{50} of 0.3 mg/kg (Figure 1A). Compound **11** also efficiently inhibited the release of IL-1β in rat hippocampus in a microdialysis experiment conducted as described previously.[14, 19] In this experiment rats were either treated with vehicle or compound **11** before stimulation with 100 mM Bz-ATP perfused via a microdialysis probe. As seen in Figure 1, compound **11** reduced the levels of released IL-1β in a dose dependent fashion from 1-10 mg/kg. Although these in vivo pharmacology results were encouraging, when human PK predictions were conducted using two different approaches, single species allometry from rat, and an in vitro/in vivo clearance extrapolation, both approaches predicted a relatively high human clearance of 13-15 mL/min/kg and a short half-life of approximately 3 h. In addition, compound **11** was found to be a moderately potent inhibitor of several cytochrome P450's, as detailed on Table 5. Allometric

scaling predicted that a 300 mg b.i.d. dosing regimen would be needed in order to maintain >50% P2X7 occupancy in human, and that this dosing schedule would result in a C_{max} of nearly 600 ng/mL. Given that robust and sustained target engagement in human is possibly required for efficacy the short predicted human half-life and CYP profile made **11** a less attractive development candidate and thus compounds with improved metabolic stability were profiled.

Figure 1. A: Ex Vivo P2X7 Occupancy for Compound **11** in Rat Brain: Concentration-Response After s.c. Administration[a] and B: Inhibition of IL-1β Release in Rat Hippocampus.

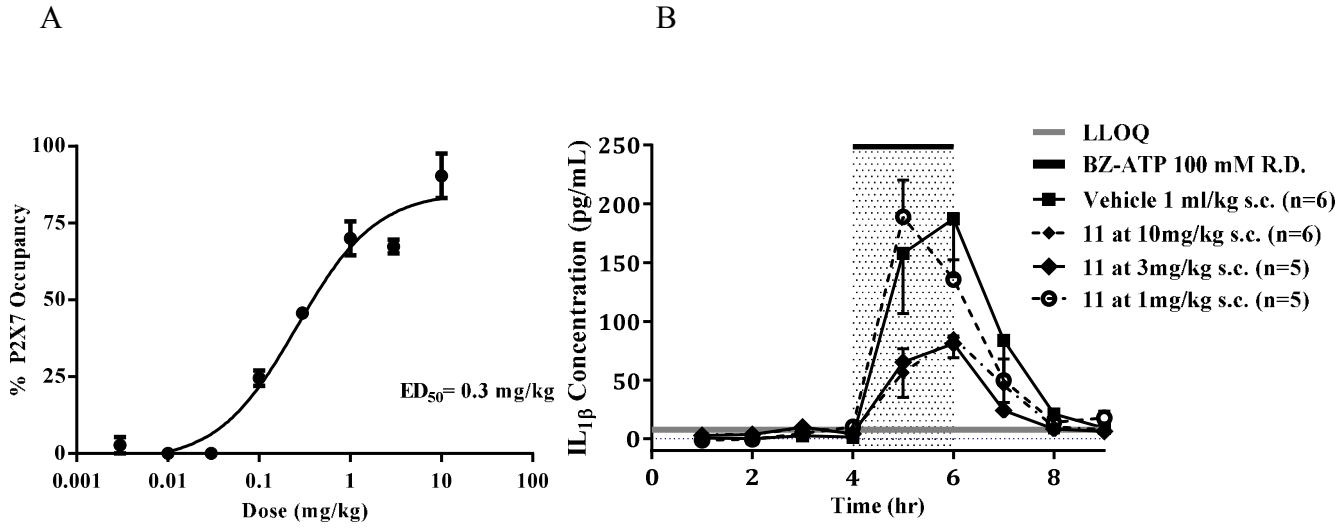

[a]Data collected 60 minutes post-dose (n=3). LLOQ = lower limit of quantitation.

The next compound characterized in vivo was compound **12**. Compound **12** incorporates a pyrimidine in place of the pyrazine in **11** and this change resulted in an improved CYP inhibition profile, improved solubility (data shown on Tables 3 and 5) with a similar selectivity profile when compared to **11** (using the same Eurofins-Cerep and kinase panels as was used for **10**). In the ex-vivo target engagement assay compound **12** also dose dependently occupied the P2X7 ion channel with an ED_{50} of 0.9 mg/kg (Figure 2).

Table 5. Select In Vitro Data for Compounds **10-14**.

Compd	CYP-1A2	CYP-2C19	CYP-2C8	CYP-2C9	CYP-2D6	CYP-3A4
10	>10[a]	2.1	>10	2.8	>10	>10
11	>10	4.3	>10	>10	>10	2.3
12	>10	>10	>10	>10	>10	>10
13	>10	>10	>10	>10	>10	>10
14	>10	>10	9.6	>10	>10	>10

[a]IC_{50} in μM, preliminary (Tier 1) data.

Figure 2. Ex Vivo P2X7 Occupancy for Compound **12** in Rat Brain: Concentration-Response After p.o. Administration.[a]

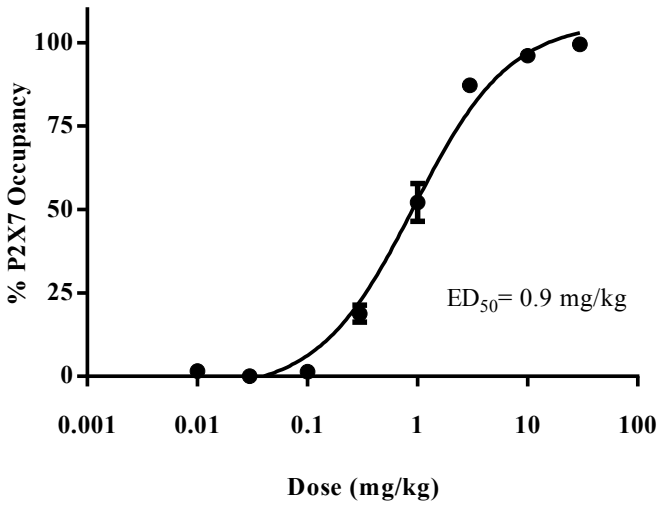

[a]Data collected 60 minutes post-dose (n=6).

The plasma concentration required for an EC_{50} in this experiment was 27 ng/mL and the brain/plasma drug ratio was found to be ~0.8. Considering the favorable target engagement data,

the pharmacokinetic properties of the compound were also assessed, in rat, dog, mouse and non-human primate. Key data are shown on Table 6.

Table 6. Rat and Dog Pharmacokinetic Parameters for Compound **12**.

Species	CL (mL/min/kg)[a]	V_{ss}(L/kg)[b]	$t_{1/2}$ (h)[c]	%F
Rat[d]	66	1.5	0.5	92%
Dog[e]	1.4	1.3	11.0	70%
Mouse[d]	32	1.1	0.4	61%
NHP[e]	19	0.9	0.8	5%

[a]Clearance, [b]volume of distribution at steady state, [c]i.v.half-life. [d]dosed at 1 mg/kg i.v. and 5 mg/kg p.o. [e]dosed at 0.5 mg/kg i.v. and 2.5 mg/kg p.o.

The PK parameters contained in Table 6 were generally in agreement with the microsomal stability data generated earlier (Table 2). However, the in vivo rat clearance was much higher than the clearance predicted by rat microsomes. Additional characterization of the metabolic fate of **12** in rat revealed that the compound was highly metabolized with only 0.4% **12** excreted unchanged. The major circulating metabolite, characterized by mass spectrometry, was consistent with the formation of (*R*)-(2-chloro-3-(trifluoromethyl)phenyl)(4-methyl-1,4,6,7-tetrahydro-5*H*-[1,2,3]triazolo[4,5-c]pyridin-5-yl)methanone resulting from loss of the pyrimidine ring. Given that this metabolic route of metabolism was more prevalent in rat than in other species, compound **12** was profiled further. Using allometry, and after correcting for differences in P2X7 affinity in human vs. rat (human pK_i=7.89 and rat $pK_{i=}$8.66) and small differences in protein binding, the estimated human dose required to maintain a trough concentration above the predicted human EC_{50} of 80 ng/mL was 100 mg q.d.

When incubated in recombinant human CYP enzymes assays, both 2C19 and 2C9 were found to be capable of metabolizing compound **12** and follow-up chemical inhibition studies in human liver microsomes suggested that CYP2C19 was the major enzyme responsible for the metabolism of **12**, which would be anticipated to increase variability in human exposure given the known polymorphisms in CYP2C19 activity.

The safety profile of compound **12** was then assessed in rats. In a rat single ascending dose toleration study **12** had only minor observations (slightly decreased activity) at 250 mg/kg, which corresponded to a plasma concentration of 175 μM. At higher doses (500 mg/kg and 1000 mg/kg) toxicological findings including decreased activity and ataxia were noted. In a rat 4-day repeated dose study (doses and exposures shown in Figure 3) there was an increased incidence and severity of hepatic lipidosis at all doses and this was associated with increased liver weights as well as signs of auto-induction at the 50 and 150 mg/kg doses. The hepatic lipidosis, which was observed at all doses, was the primary reason that compound **12** was not recommended for additional early development enabling studies.

Given the metabolism challenges with compounds **11** and **12** and the possibly related hepatotoxicity, one approach that was taken to reduce the hepatic lipidosis was to modify the heteroaromatic substituent on the triazole in order to redirect or reduce metabolism via a presumed dearylation sequence. As such, among many others, compounds **13** and **14** were prepared and characterized. The hypothesis was the 4-methylpyrimidine present in **13** might change the metabolic fate of this compound towards oxidation of the methyl group and that the 5-fluoropyrimidine present in **14** would be less susceptible to oxidation as compared to the corresponding unsubstituted pyrimidine present in **12**.

Figure 3. Plasma Exposures in the Rat Multiple Ascending Dose Study for Compound **12** (administered p.o.).

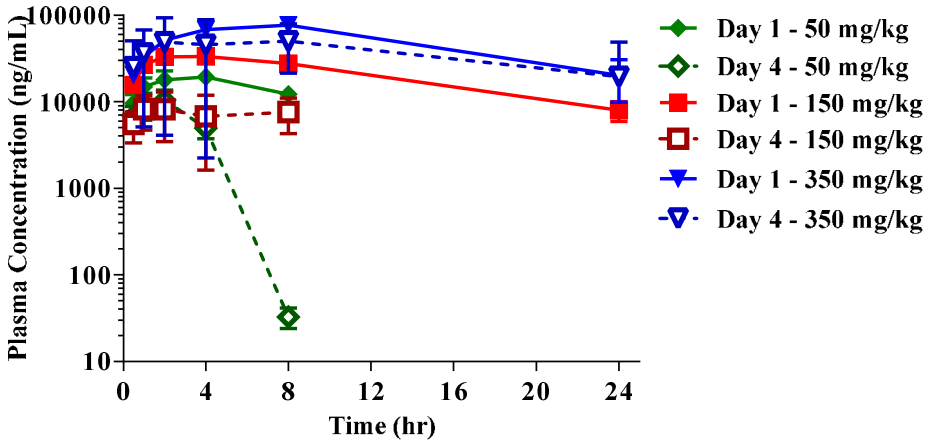

In keeping with our hypothesis, compounds **13** and **14** were generally more stable in liver microsomes than the previous compounds (Table 3). The major metabolite observed with **13** was oxidation of the methyl group on the pyrimidine and the 5-fluoropyimidine **14** was remarkably stable in both microsomes and hepatocytes. PK data for compound **13** in rat and dog are shown on Table 7.

Compound **13** had high clearance in rat and a very poor bioavailability however the dog PK was predicted by microsomal turnover and the human PK for this compound was expected to be suitable, and thus a target engagement experiment was completed for **13**. In an ex vivo P2X7 occupancy assay in rat **13** effectively occupied the channel with an ED_{50} of 8.3 mg/kg, which is significantly higher than that measured with compounds **11** and **12**, likely due to the poor rat PK.

Table 7. Rat and Dog Pharmacokinetic Parameters for Compound **13**.

Species	CL (mL/min/kg)[a]	V_{ss}(L/kg)[b]	$t_{1/2}$ (h)[c]	%F
Rat[d]	64	1.6	0.8	3%
Dog[e]	21	1.8	0.7	86%

[a]Clearance, [b]volume of distribution at steady state, [c]i.v.half-life. [d]dosed at 1 mg/kg i.v. and 5 mg/kg p.o. [e]dosed at 0.5 mg/kg i.v. and 2.5 mg/kg p.o.

The plasma EC_{50} measured in this experiment for **13** was 51 ng/mL, which is consistent with the values measured for previous compounds. This data allowed for a human PK prediction and preliminary estimates indicated that **13** would have a human half-life of around 3 hours and 100 mg b.i.d. would be required for sustained P2X7 occupancy. Compound **13** was tested in a 4-day repeated dose toleration study at doses of 50, 125 and 500 mg/kg/day in rats. Auto-induction, associated with increased liver weight, was observed in that study. Given the relatively high predicted human dose needed for target engagement, preliminary data indicating that **13** was also metabolized by the polymorphic 2C19 CYP, and the favorable data that were being generated for compound **14**, the progression of compound **13** was halted at this time.

In vitro characterization of compound **14** is detailed on Tables 1-3. The compound is potent, stable in liver microsomes and has an acceptable protein binding profile. Compound **14** was also screened in a commercial panel of 50 ion channels, receptors and transporters (Eurofins-CEREP, http://www.eurofins.com/) (tested at 10 μM), a kinase panel (tested at 1 μM) and a panel of related P2X receptors (P2X1, P2X2, P2X3, P2X2/3 and P2X4 FLIPR assays, tested up to 10 μM) and no significant activity was detected. The compound is highly permeable and has no evidence of efflux as measured by a Caco-2 cell line (A to B P_{app} = 75.3 x 10^{-6} cm^{-1}/sec, B to A

P_{app} = 48.8 x 10^{-6} cm^{-1}/sec). Compound **14** efficiently binds to recombinant rat and human P2X7 and to native tissues in both human and rat (human peripheral blood monocytes, human whole blood and rat cortex) as shown on Table 8. The compound also inhibited P2X7 activity in human, rat, dog, mouse and macaque Ca^{2+} flux assays and inhibited IL1-β release in human peripheral blood monocytes (pIC_{50} of 7.7±0.1) and in human whole blood (pIC_{50} of 8.1±0.1).

Table 8. Additional In Vitro Data for Compound **14**.

Species	P2X7 FLIPR[a]	P2X7 binding[b]	Blood[a]	cortex
Rat	8.46±0.36[c]	8.3±0.05	n.t.	8.0±0.1
Human	8.81±0.24[c]	8.3±0.1	8.1±0.2	n.t.
Mouse	7.8±0.1	n.t.	7.5±0.2	n.t.
Dog	7.9±0.1	n.t.	6.8±0.06	n.t.
Macaque	8.1±0.1	n.t.	n.t.	n.t.

[a]pIC_{50}. [b]pK_i. [c]data from Table 1.

Target engagement in rat was also demonstrated for compound **14** utilizing ex-vivo autoradiography as was done with previous compounds. Compound **14** showed dose-dependent occupancy in this experiment as shown on Figure 4. The measured ED_{50} was 0.46 mg/kg, which corresponded to a plasma EC_{50} of 105 ng/mL.

This compound has a brain/plasma ratio of approximately 1.1 in rat. As is also shown on Figure 4, compound **14** has robust and sustained P2X7 occupancy in the rat following a 10 mg/kg p.o. dose (>80% occupancy for 24 h). Given the excellent target engagement data for compound **14**, the low metabolic turnover in liver microsomes (Table 2) and the lack of CYP inhibition (Table

5) the compound was extensively characterized in vivo. Details of the PK in rat, dog and NHP are shown on Table 9.

Figure 4. Ex Vivo P2X7 Occupancy for Compound **14** in Rat: Concentration-Response After p.o. Administration[a] (n=3) and Time Course for Occupancy after a 10 mg/kg p.o. Dose in Rat (n=3).

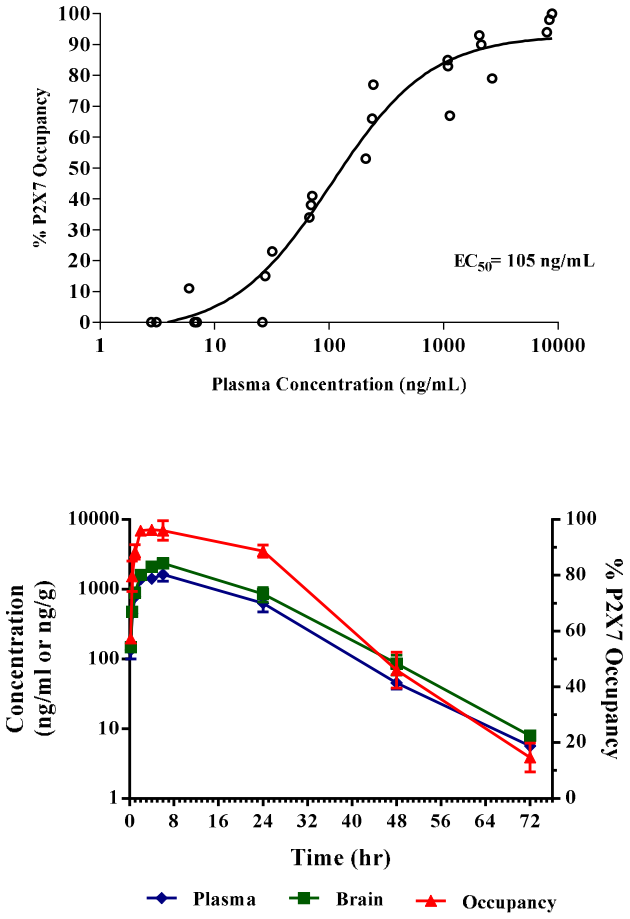

As predicted by liver microsomes compound **14** has very low clearance in all species and high bioavailability. Using this data, three species allometry allowed for a prediction of the human pharmacokinetic parameters for **14**.

Table 9. Rat and Dog Pharmacokinetic Parameters for Compound **14**.

Species	CL (mL/min/kg)[a]	V_{ss}(L/kg)[b]	$t_{1/2}$ (h)[c]	%F
Rat[d]	2.9	2.1	8.6	96%
Dog[e]	0.9	2.5	32	164%
NHP[e]	4.4	2.1	6.9	157%

[a]Clearance, [b]volume of distribution at steady state, [c]i.v.half-life. [d]dosed at 1 mg/kg i.v. and 5 mg/kg p.o. [e]dosed at 0.5 mg/kg i.v. and 2.5 mg/kg p.o.

This analysis predicted very low clearance in human (0.6 mL/kg) and a moderate V_{ss} of 1.4 L/kg. Using these parameters, the human half-life was predicted to be 29 h and the dose required to maintain >50% occupancy over 24 h was estimated to be 8 mg q.d. with the assumption of 100% bioavailability. The robust rat target engagement data and human dose prediction for **14** prompted a decision to progress **14** into more extensive pre-clinical characterization.

In rat and human brain sections, **14** concentration dependently blocked the binding of [^{3}H]- (6S)-7-[[2-chloro-3-(trifluoromethyl)phenyl]methyl]-6-methyl-3-pyrimidin-2-yl-5,6-dihydro-[1,2,4] triazolo[4,3-a]pyrazin-8-one (**15**)[26] as shown on Figure 5. Compound **14** also dose dependently inhibited the release of IL-1β in rat hippocampus after oral administration as shown on Figure 6.[19] Attempts to correlate P2X7 occupancy or inhibition of IL-1β release in rat brain with inhibition of IL-1β release in rat blood failed due to the fact that rat blood does not release measurable IL-β after stimulation with Bz-ATP.

As such, in order to establish a relationship between P2X7 occupancy in brain and IL-1β release in blood dogs were dosed orally with **14** and blood and brain samples were taken at various time

points. Drug levels in blood and brain were measured, the inhibition of ex vivo release was measured in blood, and the level of P2X7 occupancy was measured ex vivo in brain.

Figure 5. Specific Binding of **14** to P2X7 Receptors in Rat and Human Brain Sections.[a]

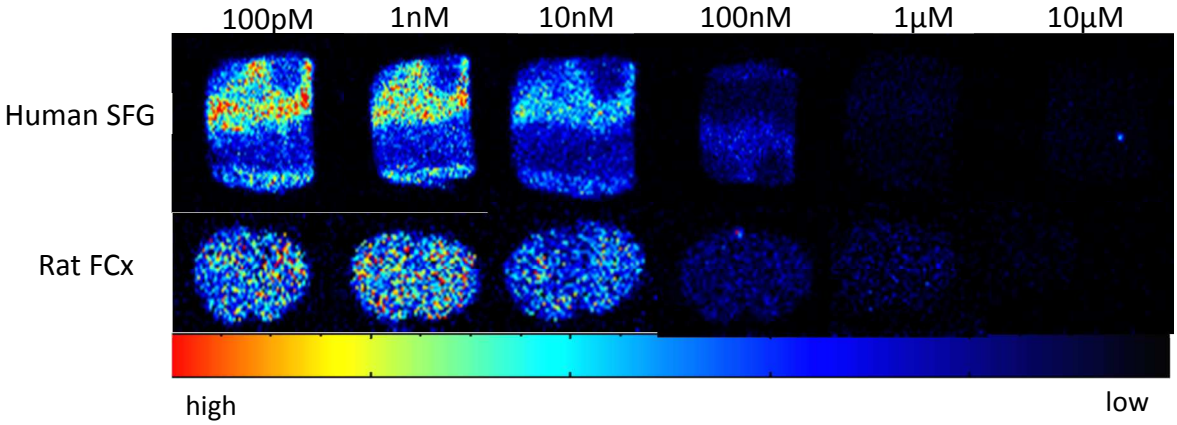

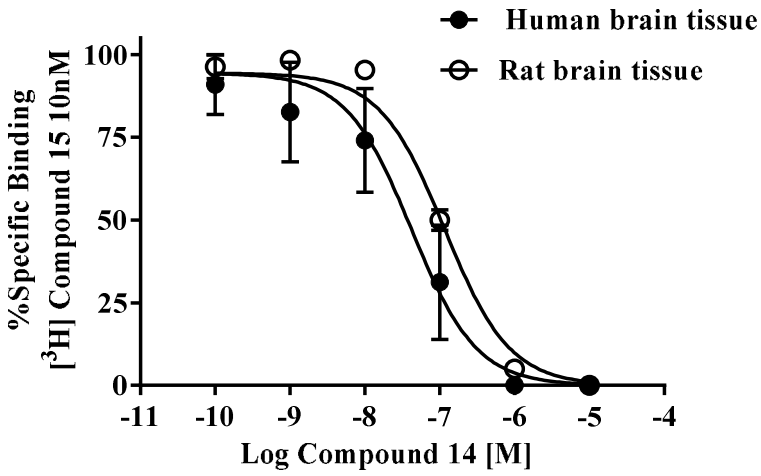

[a]FCx = frontal cortex, SFG = superior frontal gyrus (n=3).

The data are shown on Figure 7. In this experiment a rather high dose of **14** (3 mg/kg) was selected in order to achieve a high level of occupancy. Given the long dog half-life of **14** the timepoints chosen for analysis were 4 h, 24 h, 96 h and 168 h post-dose. In this preliminary

experiment robust inhibition of IL-1β release in blood was observed at the 4 h, 24 h and 96 h timepoints and this correlated well with drug levels measured in blood and the potency of **14** in dog blood in an in vitro assay (Table 8).

Figure 6. Inhibition of IL-1β Release in Rat Hippocampus After Oral Administration of Compound **14**.

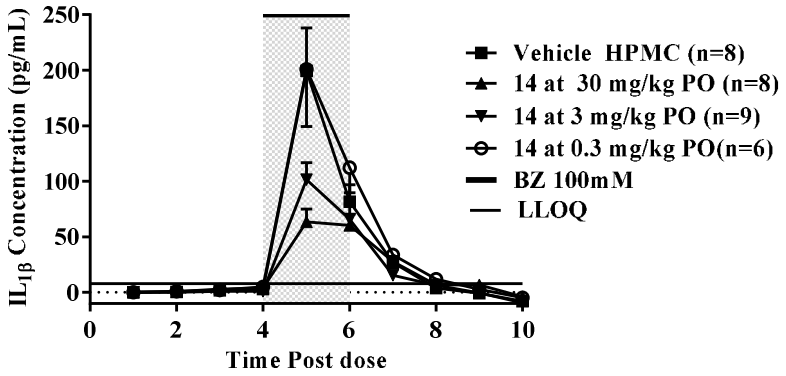

By the 168 h timepoint drug levels were reduced to 500 nM or less which is consistent with the pharmacology of **14** in dog. In addition, P2X7 brain occupancy of compound **14** was assessed by ex vivo autoradiography. As shown in Figure 7, full P2X7 brain occupancy was observed for 96 h post dose with brain exposures > 1 μM, again consistent with the pharmacology of the compound. Similar to the blood IL-1β data, drug levels started to fall at 168 h in the brain as well, with concomitant drop in occupancy. Although more experiments are needed (for example a dose response) to definitively establish a stronger correlation between IL-1β release in blood and P2X7 target engagement in the CNS, this preliminary experiment indicates that a human whole blood IL-1β assay might be a useful proxy for predicting CNS P2X7 target engagement in the clinic.

Figure 7. Central and Peripheral Target Engagement Study for **14** in Dog (3 mg/kg p.o.).[a]

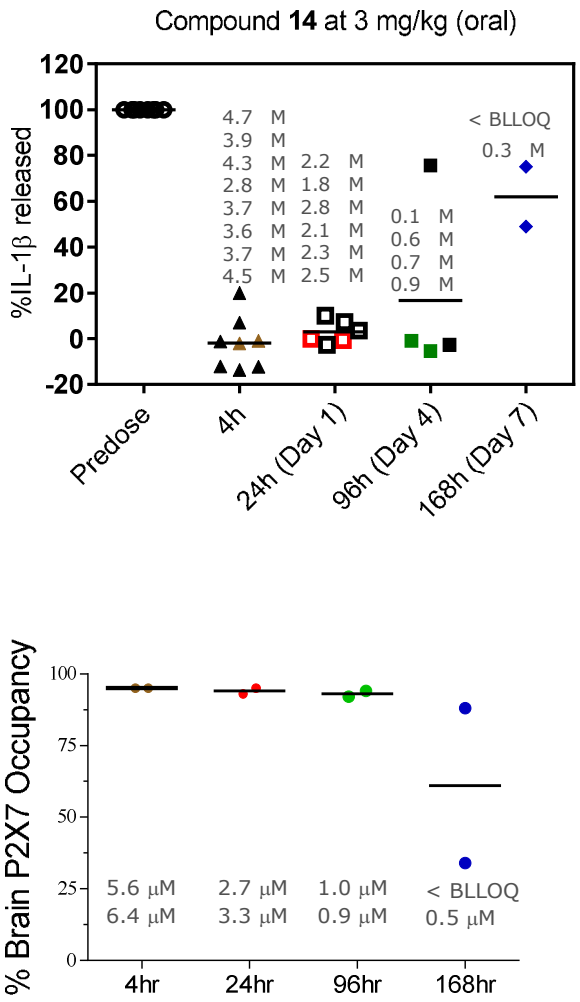

[a] Blood was used to determine IL-1β release by ex vivo stimulation of LPS and Bz-ATP. Brains were collected and level of P2X7 receptor occupancy was measured by ex vivo receptor occupancy. Plasma and brain samples were also used to determine exposure of **14**.

Toleration studies in rat and dog were also completed for **14**. In rat, the compound was evaluated in a four day study at doses of 62.5, 125 and 250 mg/kg. No significant clinical observations were noted in this study and exposures were high at all doses. The exposure data are shown in Figure 8. In a dog five day toleration study at doses of 30, 100 and 300 mg/kg exposures were also high and no relevant changes in serum chemistry, necropsy or histopathology were observed.

Figure 8. Plasma Concentrations of **14** in a Rat Toleration Study on Day 1 and Day 4 (oral administration, n=3).

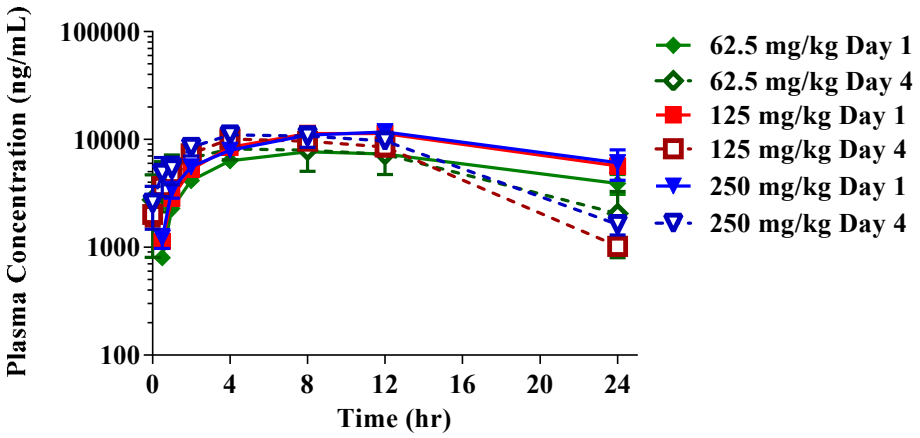

Given that **14** had excellent PK in multiple species, a very low predicted human efficacious dose and an excellent pre-clinical safety profile, the compound was nominated for clinical development and has since been dosed in healthy volunteers at single doses from 0.5 mg to 600 mg. All doses were well tolerated. The details of clinical studies with **14** will be published in due course.

CHEMISTRY

The medicinal chemistry synthesis used to prepared the 4-(*R*)-methyl-6,7-dihydro-4*H*-triazolo[4,5-c]pyridines is shown in Scheme 1. A Pd catalyzed reaction of 4-chloro-3-nitropyridine with an aniline[27] formed the aminopyridines **16** and subsequent Pd catalyzed hydrogenation provided the diamines **17** which were then treated with *t*-butyl nitrite to give the triazolopyridines **18**. Reaction with 2-chloro-3-(trifluoromethyl)benzoyl chloride presumably formed the acyl-pyridinium species which when treated *in-situ* with methyl magnesium bromide formed the (2-chloro-3-(trifluoromethyl)phenyl)(4-methyl-1-aryl-1,4-dihydro-5*H*-[1,2,3]triazolo[4,5-c]pyridin-5-yl)methanones **19**.[28]

Reduction to obtain the 4-methyl-6,7-dihydro-4*H*-triazolo[4,5-c]pyridines **20** was accomplished via transfer hydrogenation using ammonium formate and Pd catalysis or using Pd/C and H_2 gas. In this reaction varying amounts of the de-chlorinated products **21** were also generated. The racemic mixtures **20** were then purified by chiral SFC to provide the desired 4-(*R*)-methyl-6,7-dihydro-4*H*-triazolo[4,5-c]pyridines **10**-**12**. The synthesis of compound **13** was completed via the addition of methyl magnesium bromide to compound **12** and oxidation with DDQ to form the methyl pyrimidine **13** as shown in Scheme 1. Compound **14** was prepared from 4-chloro-2-methyl-3-nitropyridine **23** in a very similar sequence.

Scheme 1. Synthesis of 4-(*R*)-methyl-6,7-dihydro-4*H*-triazolo[4,5-c]pyridines **10-14**.[a]

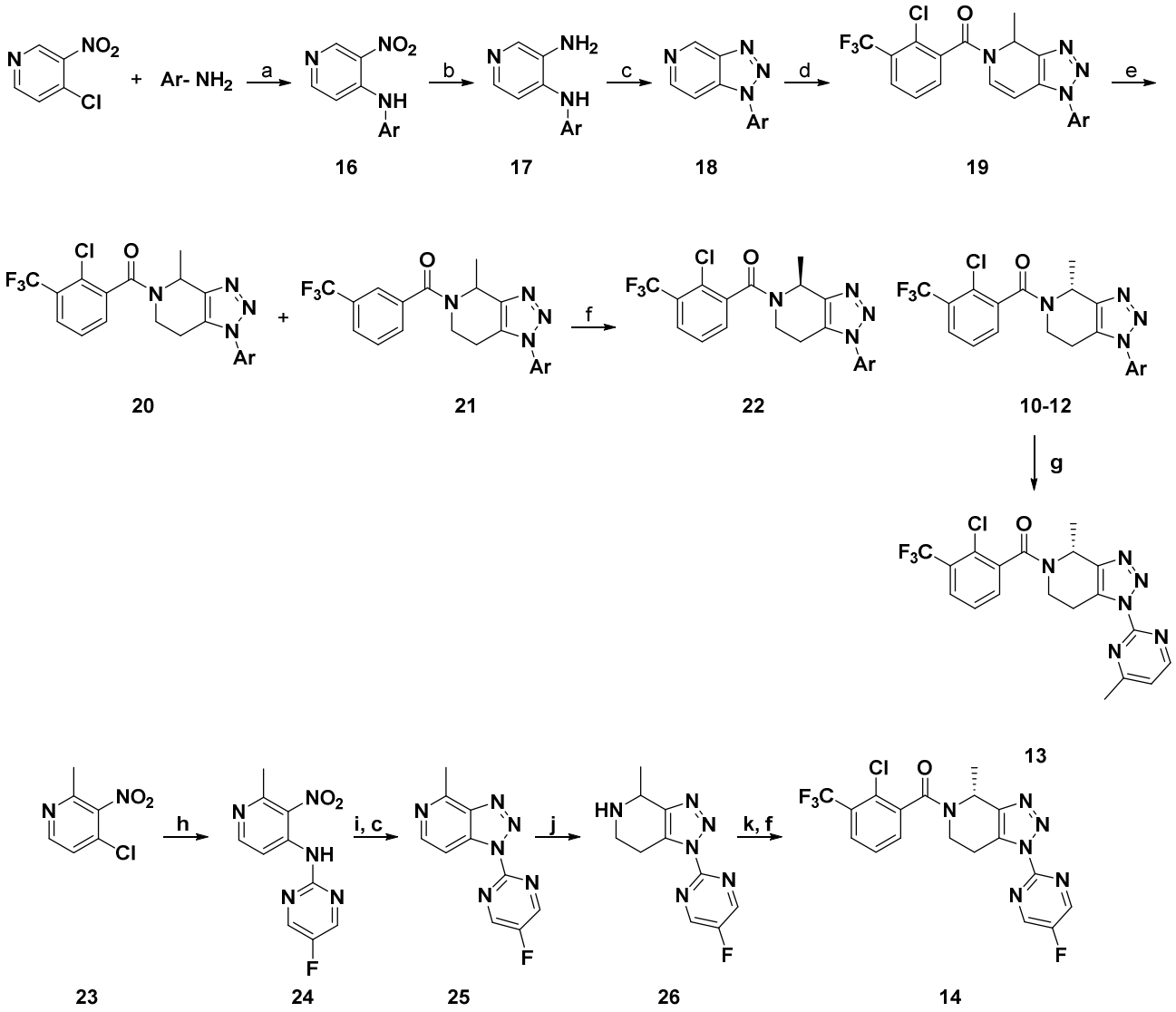

[a]Reagents and Conditions: (a) $Pd(OAc)_2$, BINAP, K_2CO_3, toluene, reflux, 38-90%, (b) H_2, Pd/C, EtOH, r.t., 80-99%, (c) *t*-BuONO, HOAc, THF, r.t., 70-90%, (d) 2-chloro-3-(trifluoromethyl)benzoyl chloride, THF, r.t., then methyl magnesium bromide, THF, -45 to -10 °C, (e) catalyst, H_2 or ammonium formate, MeOH or HOAc, (f) SFC, (g) methyl magnesium bromide, THF, 0 to 23 °C, then THF/H_2O/HOAc, DDQ, 0 to 23 °C, 81%, (h) $Pd(OAc)_2$, DINAP,

2-amino-4-fluoropyridine, K_2CO_3, toluene, 110 °C, 38%, (i)10%Pd/C, H_2, EtOH, HOAc, 88%, (j) 10% Pt/C, HOAc, H-Cube, 60 bar, 60 °C, 51%, (k) 2-chloro-3-(trifluoromethyl)benzoic acid, HATU, Et_3N, DMF, 23 °C, 90%.

X-ray crystallography was used to determine the absolute configuration of compound **14** using anomalous dispersion as shown on Figure 9 and confirms the (*R*)-configuration.

Figure 9. Ball and Stick Diagram Depicting the X-Ray Crystal Structure of **14**.[a]

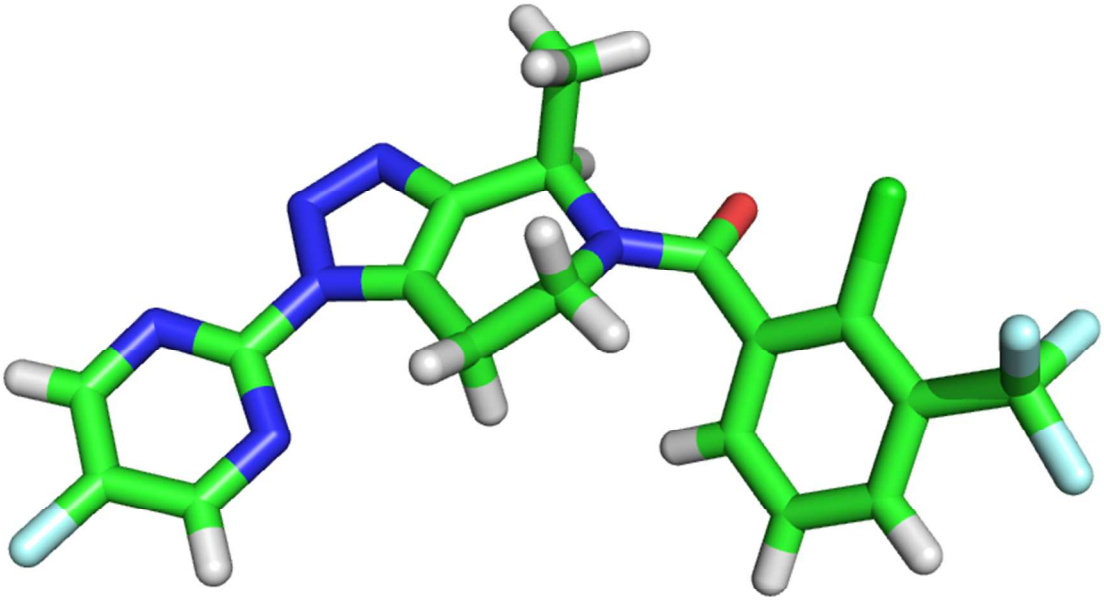

[a]The asymmetric unit contains one fully ordered molecule of **14**.

CONCLUSION

Optimization of the pharmacokinetic properties of several lead series of P2X7 antagonists led to the identification of the 4-(*R*)-methyl-6,7-dihydro-4*H*-triazolo[4,5-c]pyridines, which are potent and selective, brain penetrant and CNS active P2X7 antagonists. The first few compounds in this series had some challenges, including PK challenges that resulted in high dose predictions in human. These compounds also had issues in toleration studies that halted their progression. Several approaches were adopted in order to reduce metabolism and therefore lower the predicted dose in human and this work ultimately resulted in the identification of compound **14** (JNJ-54175446) as a potential clinical candidate for the treatment of mood disorders. Compound **14** entered the early development portfolio and has been dosed in healthy volunteers and was well tolerated.

EXPERIMENTAL SECTION

Chemistry. General Methods. The following experimental and analytical protocols were followed unless otherwise indicated. Anhydrous solvents were obtained from a GlassContour solvent dispensing system. Unless otherwise stated, reaction mixtures were magnetically stirred at room temperature (rt) under a nitrogen atmosphere. Where solutions were "dried," they were dried over a drying agent such as Na_2SO_4 or $MgSO_4$. Where mixtures, solutions, and extracts were "concentrated", they were typically concentrated on a rotary evaporator under reduced pressure. Reactions under microwave irradiation conditions were carried out in a Biotage Initiator or CEM Discover instrument. Normal-phase silica gel column chromatography (sgc) was performed on silica gel (SiO_2) using prepackaged cartridges, eluting with 2 M NH_3/MeOH in CH_2Cl_2 or EtOAc in Hexanes unless otherwise indicated. Preparative reverse-phase high

performance liquid chromatography (HPLC) was performed on a Agilent HPLC with an XBridge™ Prep C18 OBD™ (5 µm, 30 x 100 mm or 50 x 100 mm) column or, and a gradient of 10 to 99% acetonitrile/water (20 mM NH_4OH) over 12 to 18 min, and a flow rate of 30 mL/min or 80 mL/min. Occasionally preparative reverse-phase high performance liquid chromatography (HPLC) is referred to as basic HPLC in the text. Preparative reverse-phase high performance liquid chromatography under acidic conditions (acidic HPLC) was performed using a Gilson HPLC with an Inertsil ODS-3 C18, 3µm 30x100mm column at 45 ºC, an acetonitrile/water with 0.05% TFA gradient over 7 min, and a flow rate of 80 mL/min. Mass spectra (MS) were obtained on an Agilent series 1100 MSD using electrospray ionization (ESI) in positive mode unless otherwise indicated. High resolution mass spectrometry data were obtained with a Bruker µTOf detector in positive mode, a Zorbax SB-C18 3.5 µM, 2.1 x 50 mm column at 40 °C, an acetonitrile/water with 0.05% formic acid gradient over 7 min, and a flow rate of 0.3 mL/min. All final compounds were determined to be >95% pure using this method. Calculated (calcd.) mass corresponds to the exact mass. Nuclear magnetic resonance (NMR) spectra were obtained on Bruker model DRX spectrometers. The format of the ^{1}H NMR data below is: chemical shift in ppm downfield of the tetramethylsilane reference (multiplicity, coupling constant J in Hz, integration). Chemical names were generated using ChemDraw Ultra 6.0.2 (CambridgeSoft Corp., Cambridge, MA) or ACD/Name Version 9 (Advanced Chemistry Development, Toronto, Ontario, Canada). Reagents were purchased from commercial suppliers and were used without purification unless otherwise noted.

The following procedures were used to prepare compounds **10**-**14**. The compounds related to generic structure **17** were prepared as described previously.[22]

(*R*)-(2-chloro-3-(trifluoromethyl)phenyl)(1-(4-fluoropyridin-2-yl)-4-methyl-6,7-dihydro-1*H*-

[1,2,3]triazolo[4,5-c]pyridin-5(4*H*)-yl)methanone (**10**).

Step 1. A suspension of 1-(4-fluoropyridin-2-yl)-1*H*-[1,2,3]triazolo[4,5-c]pyridine (200 mg, 0.93 mmol) in THF (5 ml) was treated with 2-chloro-3-(trifluoromethyl)benzoyl chloride (248 mg, 1.02 mmol) and the reaction was stirred for 10 min. The reaction was then cooled to 0º C and methyl magnesium bromide (0.34 mL, 1.0 M in THF) was added dropwise. The reaction mixture was then allowed to warm to 23 °C and stirred overnight. The reaction mixture was quenched with $NaHCO_3$ and extracted with EtOAc. The organic extracts were separated, dried (Na_2SO_4), the solvent concentrated in vacuo. The crude product was purified by chromatography (silica, EtOAc in heptane 50:50 to 70:30), the desired fractions were collected, the solvent evaporated, to give a solid that was washed with diethyl ether/DIPE to give 2-chloro-3-(trifluoromethyl)phenyl-(1-(5-fluoropyridin-2-yl)-4-methyl-1*H*-[1,2,3]triazolo[4,5-c]pyridin-5(4*H*)-yl)methanone as a white solid (130 mg, 32%). 96.3% pure by LCMS.

Step 2. 2-chloro-3-(trifluoromethyl)phenyl-(1-(4-fluoropyridin-2-yl)-4-methyl-1*H*-[1,2,3]triazolo[4,5-c]pyridin-5(4*H*)-yl)methanone (200 mg, 0.46 mmol) dissolved in acetic acid (10 mL) was subjected to a hydrogen atmosphere on a Thales Nano hydrogenation apparatus using Rh/C as the solid support at 80 PSI at 80 °C and at a flow rate of 1 ml/min. The solvent was then evaporated and the remaining materials were diluted with DCM and washed with Satd. Na_2CO_3. The organic phase was separated, dried (Na_2SO_4), and the solvent was evaporated in vacuo. The crude product was purified by chromatography (silica, EtOAc in heptane from 40:60 to 70:30), the desired fractions were collected, and the solvent was evaporated to give (2-chloro-3-(trifluoromethyl)phenyl)(1-(5-fluoropyridin-2-yl)-4-methyl-6,7-dihydro-1*H*-[1,2,3]triazolo[4,5-c]pyridin-5(4*H*)-yl)methanone (racemic **10**) as a white foam. 99.3% pure by LCMS.

Step 3. The racemic material obtained in Step 2 was purified by chiral SFC using a Chiralcel OD-H 5μm 250x20mm column and a mobile phase of 80% CO_2 and 20% EtOH containing 0.3% *i*$PrNH_2$ to obtain compound **10**. Purity was confirmed by analytical SFC using a CHIRALCEL OD-H (250x4.6mm) and a mobile phase of 80% CO_2, 20% EtOH containing 0.3% i$PrNH_2$ over 7 minutes. (100% single enantiomer, 3.43 min retention time). MS (ESI): mass calculated for $C_{19}H_{14}ClF_4N_5O$, 439.1; m/z found, 439.9 $[M+H]^+$. ^{1}H NMR (400 MHz, $CDCl_3$), mixture of 4 rotamers 35:25:25:15, δ ppm 1.49 (d, *J* = 6.7 Hz, 0.75 H), 1.57 (d, *J* = 6.7 Hz, 0.45 H), 1.69 (d, *J* = 6.9 Hz, 0.75 H), 1.71 (d, *J* = 6.7 Hz, 1.05 H), 2.96 - 3.68 (m, 3.6 H), 4.76 (q, *J* = 6.9 Hz, 0.25 H), 4.87 (q, *J* = 6.7 Hz, 0.15 H), 5.09 - 5.17 (m, 0.4 H), 6.06 (q, *J* = 6.7 Hz, 0.35 H), 6.08 (q, *J* = 6.9 Hz, 0.25 H), 7.04 - 7.14 (m, 1 H), 7.28 - 7.32 (m, 0.15 H), 7.41 (t, *J* = 7.5 Hz, 0.15 H), 7.45 - 7.58 (m, 1.7 H), 7.75 - 7.81 (m, 1 H), 7.88 - 7.97 (m, 1 H), 8.40 (dd, *J* = 8.1, 5.5 Hz, 0.35 H), 8.43 (dd, *J* = 8.1, 5.5 Hz, 0.25 H), 8.47 - 8.52 (m, 0.4 H). HRMS calcd for $C_{19}H_{14}ClF_4N_5O$ $[M + H]^+$ 440.0896, observed 440.0886. $[\alpha]_D$ = -23.2 (c=0.56, DMF).

(*R*)-(2-chloro-3-(trifluoromethyl)phenyl)(4-methyl-1-(pyrazin-2-yl)-1,4,6,7-tetrahydro-5*H*-[1,2,3]triazolo[4,5-c]pyridin-5-yl)methanone (**11**).

Step 1. A suspension of 1-pyrazin-2-yl-1*H*-[1,2,3]triazolo[4,5-c]pyridine (100 mg, 0.5 mmol) in THF (2.5 mL) was treated with 2-chloro-3-(trifluoromethyl)benzoyl chloride (135 mg, 0.56 mmol) and the reaction was stirred for 10 min at 23 °C. The reaction was cooled to -50 °C and treated with methyl magnesium bromide (3.0 M solution in Et_2O, 0.18 mL, 0.56 mmol), and then slowly warmed to 23 °C over 30 minutes. Saturated $NaHCO_3$ solution was added to the reaction mixture, which was then extracted with EtOAc and purified on 16 g SiO_2 with 0-50% ethyl acetate/hexanes to provide 174 mg (82%) of (2-chloro-3-(trifluoromethyl)phenyl)(4-methyl-1-(pyrazin-2-yl)-1,4-dihydro-5*H*-[1,2,3]triazolo[4,5-c]pyridin-5-yl)methanone. MS (ESI): mass

calcd. for $C_{18}H_{12}ClF_3N_6O$, 420.1; m/z found, 421.1 $[M+H]^+$. ^{1}H NMR (400 MHz, $CDCl_3$) δ 9.64 – 9.45 (t, J = 1.8 Hz, 1H), 8.75 – 8.58 (d, J = 2.6 Hz, 1H), 8.51 – 8.38 (ddd, J = 6.8, 2.6, 1.5 Hz, 1H), 7.95 – 7.78 (dt, J = 4.5, 1.8 Hz, 1H), 7.70 – 7.38 (m, 2H), 6.69 – 6.54 (m, 1H), 6.44 – 6.22 (m, 2H), 1.70 – 1.50 (m, 4H).

Step 2. A suspension of (2-chloro-3-(trifluoromethyl)phenyl)(4-methyl-1-(pyrazin-2-yl)-1,4-dihydro-5*H*-[1,2,3]triazolo[4,5-c]pyridin-5-yl)methanone (150 mg, 0.36 mmol) in MeOH (3.0 mL) and THF (1.0 mL) was treated with 10% Pd/C (30 mg), subjected to an atmosphere of H_2 and stirred overnight. The reaction was filtered through celite and purified on 12 g SiO_2 with 0-70% EtOAc/ DCM to give (2-chloro-3-(trifluoromethyl)phenyl)(4-methyl-1-(pyrazin-2-yl)-1,4,6,7-tetrahydro-5H-[1,2,3]triazolo[4,5-c]pyridin-5-yl)methanone (racemic **11**). MS (ESI): mass calcd. for $C_{18}H_{14}ClF_3N_6O$, 422.1; m/z found, 423.1 $[M+H]^+$.

Step 2 (alternative procedure). To a suspension of (2-chloro-3-(trifluoromethyl)phenyl)(4-methyl-1-(pyrazin-2-yl)-1*H*-[1,2,3]triazolo[4,5-c]pyridin-5(4*H*)-yl)methanone (3 g, 7.13 mmol) in MeOH (140 mL) was added ammonium formate (2 g, 31.718 mmol) and Johnson Mathey 5% Pd/Al_2O_3 (0.5 g, 4.7 mmol). The reaction mixture was heated to reflux for 45 minutes. The reaction was cooled to room temperature then filtered through a pad of celite. The filtrate was concentrated to a solid that contained a mixture of **11** and (4-methyl-1-(pyrazin-2-yl)-1,4,6,7-tetrahydro-5*H*-[1,2,3]triazolo[4,5-c]pyridin-5-yl)(3-(trifluoromethyl)phenyl)methanone which was then purified by silica gel chromatography (3 times) using 4/1 EtOAc/hexane to obtain (2-chloro-3-(trifluoromethyl)phenyl)(4-methyl-1-(pyrazin-2-yl)-1,4,6,7-tetrahydro-5*H*-[1,2,3]triazolo[4,5-c]pyridin-5-yl)methanone (racemic **11**) (2.1 g, 70%).

Step 3. The racemic material obtained in Step 2 was purified by chiral SFC using a CHIRALPAK AD-H 5μm, 250x20mm column and a mobile phase of 75% CO_2, 25% EtOH to obtain compound **11**. The enantiomeric purity was confirmed by analytical SFC using a CHIRALPAK AD-H (250x4.6mm) and a mobile phase of 70% CO_2, 30% EtOH containing 0.3% *i*$PrNH_2$ over 7 minutes. (100% single enantiomer, 2.57 min retention time). MS (ESI): mass calcd. for $C_{18}H_{14}ClF_3N_6O$, 422.1; m/z found, 423.1 $[M+H]^+$. ^{1}H NMR (400 MHz, $CDCl_3$) δ 9.59 – 9.44 (m, 1H), 8.71 – 8.58 (m, 1H), 8.56 – 8.35 (m, 1H), 7.90 – 7.69 (m, 1H), 7.69 – 7.29 (m, 2H), 6.08 (dt, J = 13.2, 6.5 Hz, 0.6H), 5.14 (dd, J = 12.8, 5.7 Hz, 0.4H), 4.96 – 4.71 (m, 0.4H), 3.70 – 2.96 (m, 3.6H), 1.79 – 1.44 (m, 3H). HRMS calcd for $C_{18}H_{14}ClF_3N_6O$ $[M + H]^+$ 423.0942, observed 423.0957. $[\alpha]_D$ = -61.3 (c=0.31, MeOH).

(*R*)-(2-chloro-3-(trifluoromethyl)phenyl)(4-methyl-1-(pyrimidin-2-yl)-1,4,6,7-tetrahydro-5*H*-[1,2,3]triazolo[4,5-c]pyridin-5-yl)methanone (**12**).

Step 1. A suspension of 1-(pyrimidin-2-yl)-1*H*-[1,2,3]triazolo[4,5-c]pyridine (120 g, 0.605 mol, 1 equiv.), 2-chloro-3-(trifluoromethyl)benzoyl chloride (147.14 g, 0.605 mol, 1 equiv.) and triisopropylsilyl trifluoromethanesulfonate (92.77 g, 0.303 mol, 0.5 equiv.) in THF (1.8 L) was stirred for 5 hours at room temperature to form a tan solid precipitate. The reaction mixture was chilled to -45 °C then methyl magnesium bromide was slowly added in dropwise over a period of 55 minutes maintaining internal temperature between -45 and -39 °C. The reaction was allowed to slowly warm up to -10 °C. After 1.5 hours, the reaction was quenched with cold water (1 L) and DCM (500 mL) for 18 hours. Any remaining insoluble solids were filtered off. The organic layer was extracted and the aqueous layer washed with DCM (2 x 500 mL). The combined organic layers were dried with Na_2SO_4, filtered and concentrated to a crude oil. The product was precipitated out by stirring the crude in mixtures of TBME (900 mL) and hexane (50

mL) to recover solids after filtration. The procedure was repeated 2 more times to recover (2-chloro-3-(trifluoromethyl)phenyl)(4-methyl-1-(pyrimidin-2-yl)-1,4-dihydro-5*H*-[1,2,3]triazolo[4,5-c]pyridin-5-yl)methanone as a white solid (103 g, 0.245 mol, 40% yield). A mixture of rotamers was observed by NMR. ^{1}H NMR (500 MHz, $CDCl_3$) δ 8.88 – 8.86 (m, 2H), 7.85 – 7.82 (m, 1H), 7.65 – 7.45 (m, 2H), 7.41 – 7.38 (t, 1H), 6.71 – 6.64 (dd, 1H), 6.39 – 6.26 (m, 2H), 1.64 – 1.60 (m, 3H). MS-ESI (m/z): [M+H]+ calcd for $C_{18}H_{12}ClF_3N_6O$, 420.78; found, 421.0.

Step 2. To a suspension of (2-chloro-3-(trifluoromethyl)phenyl)(4-methyl-1-(pyrimidin-2-yl)-1,4-dihydro-5*H*-[1,2,3]triazolo[4,5-c]pyridin-5-yl)methanone (126 g, 0.30 mol, 1.0 equiv) in DMF (1.7 L) was added ammonium formate (151.0 g, 2.4 mol, 8 equiv.) and Johnson Mathey 5% Pd/Al_2O_3 (13.6 g). The reaction was heated to 60 °C for 7 hours then filtered. The filtrate was concentrated to 1/3 volume and quenched with H_2O (1 L). The mixture was stirred vigorously under ice bath for 18 hours to form precipitation. The solids were filtered and dried to afford 113.2 grams of *rac*-(2-chloro-3-(trifluoromethyl)phenyl)(4-methyl-1-(pyrimidin-2-yl)-1,4,6,7-tetrahydro-5*H*-[1,2,3]triazolo[4,5-c]pyridin-5-yl)methanone as tan solid. An alternative route to *rac*-(2-chloro-3-(trifluoromethyl)phenyl)(4-methyl-1-(pyrimidin-2-yl)-1,4,6,7-tetrahydro-5*H*-[1,2,3]triazolo[4,5-c]pyridin-5-yl)methanone and characterization of this compound has been published previously.[29]

Step 3. The racemic mixture obtained in Step 2 was purified by chiral SFC (Stationary phase: Chiraplpak AD 5µm 250*30mm), Mobile phase: 70% CO_2, 30% mixture of MeOH/iPrOH 50/50 v/v) to provide (*R*)-(2-chloro-3-(trifluoromethyl)phenyl)(4-methyl-1-(pyrimidin-2-yl)-1,4,6,7-tetrahydro-5*H*-[1,2,3]triazolo[4,5-c]pyridin-5-yl)methanone (49 g, 0.116 mol, 39%) as white solid. Chiral HPLC analysis: Chiral Pak AD-H column, 0.4 mL/min, 80% EtOH / 20%

hexane, R isomer 14.05 min, S isomer 10.60 min. MS-ESI (m/z): [M+H]+ calcd for $C_{18}H_{14}ClF_3N_6O$, 422.80; found, 423.10. ^{1}H NMR (500 MHz, $CDCl_3$) δ 8.80 – 8.43 (m, 2H), 7.82 – 7.44 (m, 1H), 7.27 – 7.15 (m, 2H), 6.66 – 6.60 (m, 1H), 5.95 – 4.92 (m, 1H), 3.77 – 2.54 (m, 3H), 1.74 – 1.53 (m, 3H). HRMS calcd for $C_{18}H_{14}ClF_3N_6O$ $[M + H]^+$ 423.0942, observed 423.0946. Elemental analysis: calculated C, 51.13; H, 3.34; N, 19.88: obtained C, 51.05; H, 3.47; N, 20.01. $[\alpha]_D$ = -148.8 (c=0.57, MeOH).

(*R*)-(2-chloro-3-(trifluoromethyl)phenyl)(4-methyl-1-(4-methylpyrimidin-2-yl)-1,4,6,7-tetrahydro-5*H*-[1,2,3]triazolo[4,5-c]pyridin-5-yl)methanone (**13**).

Step 1. To a solution of (R)-(2-chloro-3-(trifluoromethyl)phenyl)(4-methyl-1-(pyrimidin-2-yl)-1,4,6,7-tetrahydro-5*H*-[1,2,3]triazolo[4,5-c]pyridin-5-yl)methanone (20.6 g, 48.7 mmol) in THF (244 mL) at 0 °C was added methyl magnesium bromide (3.0 M in Et_2O, 33 mL, 97 mmol), and upon complete addition of methyl magnesium bromide the reaction mixture was warmed to room temperature and stirred for 30 min. Then, the reaction mixture was cooled to 0 °C and a 20:1:1 solution of THF/H_2O/AcOH (71 mL) was added and the resulting mixture stirred at 0 °C for 10 min. A solution of DDQ (11.6 g, 51.2 mmol) in THF (122 mL) was then added at 0 °C and the reaction mixture warmed to room temperature and stirred for 30 min. The mixture was diluted with EtOAc, washed with 1 M NaOH (3X) and brine (1X). The aqueous layer was extracted with EtOAc (2X). The combined organics were dried with Na_2SO_4, filtered and concentrated to give a brown foam, which was partially purified by silica gel chromatography (0-50% EtOAc/DCM) to give **13** (22 g), which was further purified by recrystallization from MTBE to give **13** as a white powder (17 g, 81%). MS (ESI) mass calcd. $C_{19}H_{16}ClF_3N_6O$, 436.10; m/z found, 437.1 $[M+H]^+$. ^{1}H NMR (400 MHz, CDCl3) δ 8.71 (dd, J = 5.0, 2.5 Hz, 0.5H), 8.69 - 8.64 (m, 0.5H), 7.81 - 7.73 (m, 1H), 7.58 - 7.36 (m, 2H), 7.31 - 7.27 (m, 0.3H), 7.25 - 7.20 (m,

0.7H), 6.13 - 6.02 (m, 0.5H), 5.16 - 5.10 (m, 0.4H), 4.92 - 4.85 (m, 0.1H), 4.80 - 4.75 (m, 0.3H), 3.67 - 3.11 (m, 3.3H), 3.07 - 2.95 (m, 0.4H), 2.68 – 2.67 (m, 1.3H), 2.65 (s, 0.6H), 2.63 (s, 1H), 1.72 (d, J = 6.9 Hz, 0.9H), 1.70 (d, J = 7.0 Hz, 0.6H), 1.58 (d, J = 7.1 Hz, 0.5H), 1.50 (d, J = 6.7 Hz, 0.9H). HRMS calcd for $C_{19}H_{16}ClF_3N_6O$ $[M + H]^+$ 437.1099, observed 437.1089. Elemental analysis: calculated C, 52.24; H, 3.69; N, 19.24: obtained C, 51.94; H, 4.04; N, 19.20. $[\alpha]_D$ = -45.8 (c=0.545, MeOH).

(*R*)-(2-chloro-3-(trifluoromethyl)phenyl)(1-(5-fluoropyrimidin-2-yl)-4-methyl-1,4-dihydro-5*H*-[1,2,3]triazolo[4,5-c]pyridin-5-yl)methanone (**14**).

Step 1. A solution of $Pd(OAc)_2$ (0.15 g, 0.68 mmol) and BINAP (0.42 g, 0.68 mmol) was stirred in toluene (2 mL) at rt for 10 minutes. This mixture was then added to a microwave vial which contained 4-chloro-2-methyl-3-nitropyridine (3.00 g, 16.8 mmol), 2-amino-4-fluoropyridine (2.20 g, 18.5 mmol), and K_2CO_3 (2.6 g, 18.6 mmol) in toluene (10 mL). The reaction was irradiated in a microwave apparatus at 110 °C for 1 h. The reaction was then diluted with DCM, filtered through celite, washed, and concentrated. Chromatography of the resulting residue (SiO_2; EtOAc:Hex) gave 5-fluoro-N-(2-methyl-3-nitropyridin-4-yl)pyrimidin-2-amine (1.60 g, 38%). MS (ESI): mass calculated for $C_{10}H_8ClFN_5O_2$, 249.07; m/z found 250.0 [M+H]+.

Step 2. To a solution of 5-fluoro-*N*-(2-methyl-3-nitropyridin-4-yl)pyrimidin-2-amine (4.0 g, 16.0 mmol) in degassed EtOH (100 mL) and AcOH (2mL) was added 10% Pd/C (1.70 g, 1.61 mmol) in EtOH (10 mL). The reaction was placed under a balloon of hydrogen at atmospheric pressure and allowed to stir for 12 h. The reaction was filtered through celite and washed with DCM. The organic solvent was concentrated to give *N*-(5-fluoropyrimidin-2-yl)-2-methylpyridine-3,4-

diamine (3.10 g, 88%). MS (ESI): mass calculated for $C_{10}H_{10}ClFN_5$, 219.09; m/z found 220.1 [M+H]+.

Step 3. A solution of *N*-(5-fluoropyrimidin-2-yl)-2-methylpyridine-3,4-diamine (0.50 g, 2.28 mmol) in THF (15 mL) and HOAc (0.14 mL, 2.51 mmol) was treated with t-butyl nitrite (0.45 mL, 3.42 mmol) and heated to 100 °C for 90 min. The reaction was concentrated, diluted with 1N $NaHCO_3$, and extracted with DCM (3 x 50 mL). The organic layers were combined, dried with Na_2SO_4, and concentrated. Chromatography of the resulting residue (SiO_2; EtOAc:Hex) provided 1-(5-fluoropyrimidin-2-yl)-1H-[1,2,3]triazolo[4,5-c]pyridine (0.40 g, 77%). MS (ESI): mass calcd. for $C_{10}H_7FN_6$, 230.07; m/z found, 231.1 $[M+H]^+$.

Step 4. A solution of 1-(5-fluoropyrimidin-2-yl)-4-methyl-1*H*-imidazo[4,5-c]pyridine (0.90 g, 3.91 mmol) in AcOH (50 mL) was passed through a 10% Pt/C catalyst cartridge on an H-Cube© hydrogenation apparatus at a pressure of 60 bar, a temperature of 60 °C, and a flow rate of 1 ml/min. The reaction was subsequently concentrated, diluted with 1N NaOH, and extracted with DCM (3 x 100 mL). The organic layers were combined, dried with Na_2SO_4, and concentrated. Chromatography of the resulting residue (SiO_2; MeOH (NH_3):DCM) gave 1-(5-fluoropyrimidin-2-yl)-4-methyl-4,5,6,7-tetrahydro-1H-[1,2,3]triazolo[4,5-c]pyridine. (0.47 g, 51%). MS (ESI): mass calcd. for $C_{10}H_{11}FN_6$, 234.10; m/z found, 235.0 $[M+H]^+$.

Step 5. A solution of 1-(5-fluoropyrimidin-2-yl)-4-methyl-4,5,6,7-tetrahydro-1H-[1,2,3]triazolo[4,5-c]pyridine (0.30 g, 1.28 mmol), 2-chloro-3-(trifluoromethyl)benzoic acid (0.34 g, 1.54 mmol), HATU (0.38 g, 1.28 mmol), and Et_3N (0.18 mL, 1.28 mmol) in DMF (5 mL) was stirred for 30 min. The reaction was then diluted with EtOAc (30 mL) and washed with H_2O (3 x 20 mL). The organic layers were combined, dried with Na_2SO_4, and concentrated.

Chromatography of the resulting residue (SiO_2; MeOH (NH_3):DCM) gave (2-chloro-3-(trifluoromethyl)phenyl)(1-(5-fluoropyrimidin-2-yl)-4-methyl-1,4,6,7-tetrahydro-5*H*-[1,2,3]triazolo[4,5-c]pyridin-5-yl)methanone (racemic **14**). (0.51 g, 90%). MS (ESI): mass calculated for $C_{18}H_{13}ClF_4N_6O$, 440.08; m/z found, 441.0 $[M+H]^+$. ^{1}H NMR (500 MHz, $CDCl_3$), a mixture of rotamers was observed, δ 8.80 – 8.43 (m, 2H), 7.82 – 7.44 (m, 1H), 7.27 – 7.15 (m, 2H), 6.66 – 6.60 (m, 1H), 5.95 – 4.92 (m, 1H), 3.77 – 2.54 (m, 3H), 1.74 – 1.53 (m, 3H). HRMS calcd for $C_{18}H_{13}ClF_4N_6O$ $[M + H]^+$ 441.0848, observed 441.0862.

Step 6. Compound **14** was purified by chiral SFC on using a Chiracel OD-H 5µm 250x20mm column and a mobile phase of 70% CO_2 and 30% EtOH. Compound **14** can also be prepared by the methods previously described.[30] m.p. 197°– 200° C. Elemental analysis: calculated C, 49.04; H, 2.98; N, 19.05: obtained C, 48.93; H, 3.25; N, 19.02. $[\alpha]_D$ = -161.7 (c=0.42, MeOH).

In Vitro Biology. General Methods.

P2X7 Antagonism in Human Peripheral Blood Mononuclear Cells (PBMCs) in Mouse and Human Whole Blood. Human blood was collected using a blood donor program. PBMCs were isolated from blood using a Ficoll density gradient technique. Briefly, blood was laid on Ficoll solution and centrifuged at RT for 20 minutes at 2000 rpm. The buffy layer (between red blood cells and plasma) was carefully collected by aspiration, washed with PBS and centrifuged again at 1500 rpm for 15 minutes. The resulting cell pellet was washed and plated on 96 well-plates for experiments. For the whole blood experiments, 150 µl of either mouse or human blood was platted on 96 well plates. Lipopolysaccharide (LPS) (30 ng/ml) was added to each well and incubated for 1hour. Test compounds were then added and incubated for 30 minutes. The P2X7 agonist, 2'(3')- 0-(4-benzoylbenzoyl) adenosine 5' triphosphate (Bz-ATP) was then added at a

final concentration of 0.5 mM (PBMC) or 1 mM (blood). Cells were incubated for an additional 1.5 hours. At that point, supernatant was collected and stored for IL-1β assay using manufacturer's protocol for enzyme linked immunosorbent assay (ELISA). Data was expressed as percent control, where control is defined as the difference in IL-1β release in LPS+Bz-ATP samples and LPS only samples. Data was plotted as response (% control) versus concentration to generate IC_{50} values.

P2X7 Antagonism in Recombinant P2X7 Cells: Ca^{2+}Flux. 1321Nl cells expressing the recombinant P2X7 channel were cultured in HyQ DME/(HyClone/Dulbecco's Modified Eagle Medium) high glucose supplemented with 10% Fetal Bovine Serum (FBS) and appropriate selection marker. Cells were seeded at a density of 25000 cells/well (96-well clear bottom black walled plates) in 100 µl volume/well. On the day of the experiment, cell plates were washed with assay buffer, containing (in mM): 130 NaCl, 2 KCl, 1 $CaCl_2$, 1 MgCl 2, 10 HEPES, 5 glucose; pH 7.40 and 300 mOs. After the wash, cells were loaded with the Calcium-4 dye (Molecular Device) and incubated in the dark for 60 minutes. Test compounds were prepared at 250x the test concentration in neat DMSO. Intermediate 96-well compound plates were prepared by transferring 1.2 µL of the compound into 300 µL of assay buffer. A further 3x dilution occurred when transferring 50 µL/well of the compound plate to 100 µL/well in the cell plate. Cells were incubated with test compounds and dye for 30 minutes. Calcium dye fluorescence was monitored in FLIPR as the cells were challenged by adding 50 µL/well of BzATP. The fluorescence change was measured 180 seconds after adding the agonist. Peak fluorescence was plotted as a function of test concentration to generate an IC_{50} value.

P2X7 Radioligand binding. Recombinant P2X7 1321Nl cells were collected and frozen @-80° C. On the day of the experiment, cell membrane preparations were made according to standard

published methods. The total assay volume was 100 µl: 10 µl compound (l0x)+(b) 40 µl tracer (2.5x)+50 µl membrane (2x). The tracer used for the assay was [^{3}H]-A-804598. The compound can be prepared as described in the literature (Donnelly-Roberts, D. Neuropharmacology 2008, 56 (1), 223-229). Compounds, tracer and membranes were incubated for 1 hour @ 4° C. The assay was terminated by filtration (GFB filters pre-soaked with 0.3% PEI) and washed with washing buffer (Tris-HCl 50 mM). The IC_{50} generated in the binding assay was corrected for tracer concentration and affinity of the tracer to derive at the affinity (K) of the test compounds.

DMPK. General Methods.

Caco-2 Permeability**.** Caco-2 bi-directional permeability assays were conducted at CEREP according to company's protocol. In brief, Caco-2 cells were seeded onto a 96-well Multiscreen plate™ (Millipore) at a cell density of 1 x 10^5 cells/cm^2 and cultured for at least 21 days before permeability studies were conducted. Test compounds were dissolved in DMSO and added to HBSS-HEPES, pH 7.4 culture media at a final concentration of 10 µM (1 % DMSO v/v). The working solution was applied to cells on the donor side and incubated at 37 ° C with gentle agitation for 60 and 40 min to determine the A→B and B→A permeability, respectively. Samples were extracted from the donor side at time zero and the end-point and from the receiver side at the end-point time only. Samples were then processed for LC/MS/MS analyses to determine the apparent permeability coefficient (P_{app}) of the test compound in the A→ B and B→A direction **(**Expert Opin Drug Metab. Toxicol. (2005) 1 (2): 175 – 185) as well as the percent recovery.

Plasma Protein Binding. Plasma protein binding was determined by equilibrium dialysis using the RED Device (Thermo Scientific, Rockford, IL) consisting of a Teflon base block and RED

Device inserts comprising two (sample and buffer) side-by-side chambers separated by a dialysis membrane. Compounds were prepared as 100 μM DMSO stocks and spiked into 1 mL of mouse, rat, and human plasma (Bioreclamations) to make a final concentration of 1 μM. Plasma (300 μL) was dispensed into wells separated by an 8 kDa-permeable cellulose membrane from wells containing 100 mM potassium phosphate, pH 7.4 (500 μL). Each compound was tested in triplicate. The RED devise was sealed and equilibrium was permitted for 6 h in a 37 °C incubator with gentle agitation at 100 RPM. After incubation, plasma samples were prepared by transferring 10 μL from plasma wells to 90 μL of fresh 100 mM potassium phosphate, pH 7.4, and buffer samples were prepared by transferring 90 μL from buffer wells to 10 μL of naïve plasma. In addition, a reference sample without equilibration was prepared in triplicate by mixing 10 μL of plasma containing 1 μM compound with 90 μL buffer in order to determine compound recovery from the assay. Two-volumes of 1:1 acetonitrile:methanol spiked with the internal standard phenytoin (0.2 μg/mL) were added to reference and samples. Precipitation of plasma protein binding was allowed for 15 min before reference and samples were centrifuge clarified. Supernatant (10 μL) was used for LC/MS/MS analyses.

Brain Tissue Binding. Brain tissue binding was assessed by equilibrium dialysis using the RED device similar to the procedure described for plasma protein binding. Rat brain tissue homogenate, prepared in PBS buffer, pH 7.4 (1:10, w/v), was spiked with compound DMSO stock solution to yield a final concentration of 5 μM. The dialysis was carried out in a shaking incubator at 37 °C for 5 h in triplicate. After incubation, 25 μL of homogenate or 50 μL of buffer was extracted with 50 μL of DMSO and 300 μL of acetonitrile and analyzed by LC/MS/MS using the calibration curves across an appropriate concentration range and quality control samples. The apparent unbound fraction ($f_{u,app}$) was derived from the formula:

$$fu, app = \frac{[\mathrm{A}]buffer}{[\mathrm{A}]homogenate}$$

where $[\mathrm{A}]_{homogenate}$ and $[\mathrm{A}]_{buffer}$ are the concentrations measured in the homogenate and buffer, respectively. The unbound fraction in undiluted brain ($f_{u,\ brain}$) was calculated from the formula

$$fu, brain = \frac{fu, app}{\mathrm{D} + fu, app - \mathrm{D} * fu, app}$$

where D is the dilution factor of 10. Subsequently, the percentage compound bound to brain tissue (% BTB) was calculated from the formula

$$\%\ BTB = (1 - fu, brain) * 100\ \%$$

Liver Microsomal Stability. Microsomal stability studies were conducted on a Biomek® FX Robotic Liquid Handling Workstation (Beckman Coulter, Brea, CA), which consists of a 96-channel pipette head, a 12-postion workstation deck, and a plate incubator. Test compounds (1 μM) were spiked in a reaction mix consisting of 100 mM potassium phosphate buffer (pH 7.4), 3 mM $MgCl_2$, and 0.5 mg/mL liver microsomes from mouse, rat, dog, monkey and human (BD Gentest). The reaction was brought to 37 °C and initiated by adding NADPH to a final concentration of 1 mM. After mixing on the plate-deck, 50 μL aliquots were excised from the reaction plate at 0, 5, 10, 20, 40, and 60 min and quenched with four volumes of acetonitrile spiked with 500 μg/nL of the internal standard phenytoin. Quenched plates were centrifuged at 5700 rpm for 10 min at 4 °C, and supernatant was diluted 1:3 in water before LC/MS/MS analysis. The compound half-lives were derived from plots of the ln of percent remaining compound over time to determine the intrinsic clearance. The predicted hepatic clearance was derived from the intrinsic clearance value using equations from the well-stirred model (Current

Drug Metabolism, 2008, 9, 940-951), where protein binding in plasma and microsomal proteins is assumed to be similar and the blood to plasma concentration ratio is assumed to be one. The hepatic extraction ratio (ER) was calculated by dividing the predicted hepatic clearance by species blood flow (Q), where Q is 90, 55, 31, 44, and 21.7 mL/min/kg for mouse, rat dog, monkey, and human, respectively.

Solubility in Aqueous Systems. Solubility in 30 mM phosphate buffers (pH 2 and pH 7), simulated gastric (SGF, 0.2% NaCl in 0.1 N HCl, pH 1.2) and intestinal fluids (FasSIF, 0.029 M phosphate buffer, 5 mM sodium taurocholate, and 1.5 mM lecithin, pH 6.8) was investigated. Compound was dissolved in DMSO solutions at a concentration of 10 mM and was used for the solubility experiment. DMSO solutions (20 μL) are dispensed in 96-well plates, and the solvent is removed by evaporation using a Caliper TurboVap 96 set at 30 °C and a flow rate of 40 Fh. Buffers (400 μL) of interest are added to the residual solids, and the resulting mixtures are stirred at room temperature for 3 days using magnetic stir bars. The samples are then filtered using an AcroPrep 1 mL 96 filter plate, and the supernatant is analyzed for compound concentration, against external standards.

Cocktail CYP Inhibition Assay. DMSO stocks were prepared for test compounds (10 mM) and for the assay positive controls: furafylline (CYP1A2 – 8 mM), quercetin (CYP2C8 – 12 mM), sulfaphenazole (CYP2C9 – 2 mM), *N*-3-benzyl-phenobarbital (CYP2C19 – 1.2 mM), quinidine (CYP2D6 – 0.16 mM), and ketoconazole (CYP3A – 0.16 mM). In a solution of 1:1 acetonitrile:water, stocks were diluted 10-fold and serial diluted in 2-fold increments. For test compounds, the final incubation concentrations were 10, 5, 2.5, 1.25, 0.63, and 0.3 μM. To simultaneously measure the activity of multiple CYPs in the same incubation, a cocktail probe solution was prepared that contained six substrates at the following final concentrations:

phenacetin (CYP1A2 – 50 μM), paclitaxel (CYP2C8 – 10 μM), diclofenac (CYP2C9 – 4 μM), *S*-mephenytoin (CYP2C19 – 30 μM), dextromethorphan (CYP2D6 – 3 μM), and midazolam (CYP3A – 2 μM). Human liver microsomes (BD Gentest) from a mixed donor pool were prepared in 0.1 mM potassium phosphate buffer (pH 7.4) supplemented with 3 mM $MgCl_2$ and pre-incubated for 5 min at 37 °C. Human liver microsomes (0.1 mg of protein/mL) were then mixed with the cocktail probe solution, test compounds or assay positive controls, and the reaction was initiated by the addition of NADPH (1 mM final concentration). The catalysis of probe substrates was permitted for 15 min at 37 °C and quenched in one volume of 1:1 acetonitrile:methanol mixture containing the internal standard phenytoin (0.2 μg/mL). Samples were vortexed for 2 min and centrifuged for 10 min. Supernatant (300 μL) was diluted in water (125 μL), mixed, and used for LC-MS/MS analysis. A 20-μL aliquot was analyzed for probe metabolite formation using a Shimadzu LC-20A HPLC system and a Sciex API 5000 (Applied Biosystems, Foster City, CA) mass spectrometer in the Multiple Reaction Monitoring (MRM) scan mode with electrospray ionization (ESI). The mobile phase consisted of water (A) and acetonitrile (B) both containing 0.1% formic acid. The chromatography was performed on Phenomenex Kinetex XB-C18 (2.0 x 50 mm, 5.0 μM) column using a gradient elution method (2% B from 0.0 to 0.3 min, followed by a linear increase to 50% B over 2.7 min and subsequently 95 % B for 0.1 min, and held at 95% B for an additional .0.9 min before returning back to 2% B) at a flow rate of 0.6 mL/min. The following transitions were monitored: *m/z* 152.1→110.0 (acetaminophen – CYP1A2), *m/z* 870.3→105.1 (6α-hydroxy-taxol – CYP2C8), *m/z* 312.1→230.0 (4-hydroxy-diclofenac – CYP2C9), *m/z* 235.3→150.2 (4-hydroxy-*S*-mephenytoin – CYP2C19), *m/z* 258.2→157.1 (dextrorphan – CYP2D6), *m/z* 342.2→297.1 (1-hydroxy-midazolam – CYP3A), and *m/z* 253.1→182.2 for phenytoin (internal standard). Data

were processed using Analyst software and included probe metabolite to internal standard peak area ratios electronically exported into Excel 2000 (Microsoft Corp., Seattle, WA) format.

Pharmacokinetic Studies. Single dose pharmacokinetic studies in preclinical species (male Balb/c mice, Sprague Dawley rats, beagle dogs, or cynomolgus monkeys) were conducted following iv (1 mg/kg) and po (5 mg/kg) administration as a solution in 20% hydroxypropyl-β-cyclodextrin (HP-β-CD). Blood was sampled at predose and at 0.033 (iv), 0.083 (iv), 0.25, 0.5, 1, 2, 4, 6, 8, and 24 h postdose. In dogs, instead of 6 and 8 h time points blood was drawn at 7 h. Plasma concentrations were quantitated by LC−MS/MS using a Sciex API 4000 (Applied Biosystems, Foster City, CA) mass spectrometer interfaced with a Shimadzu LC-20 AD system. Pharmacokinetic parameters were derived from noncompartmental analysis of the plasma concentration vs time data using WinNonlin software (Pharsight, Palo Alto, CA).

Toleration Studies. General Methods.

1 and 4-Day Repeat Dose Oral Toxicology Studies. For the single dose study animals were administered test compound via oral gavage with necropsy performed on the next day. For the repeat dose toxicology group animals were administered oral doses (gavage) of test compound for 4 days, with necropsy performed on day five. Clinical observations were recorded daily and at necropsy, a list of tissues from control and treated groups were embedded in paraffin, processed into slides by sectioning at 4μm, stained with hematoxylin and eosin, and examined microscopically. Organ weights of a number of organs were also determined. Clinical pathology parameters were also measured at the end of the dosing period.

ASSOCIATED CONTENT

Supporting Information.

This supporting information is available free of charge on the ACS Publications website at http://pubs.acs.org.

Molecular formula strings (CSV file).

Coordinates for the Crystal Structure of Compound 14 (PDF). The Authors will release the atomic coordinates and experimental data for **14** upon article publication.

AUTHOR INFORMATION

Corresponding Author

* (M.A.L.) e-mail: mletavic@its.jnj.com. Tel: 1-858-450-2302.

Author Contributions

Anindya Bhattacharya, Michael A. Letavic and Brad M. Savall contributed equally to this work. The manuscript was written through contributions of all authors. All authors have given approval to the final version of the manuscript.

ACKNOWLEDGEMENTS

The authors gratefully acknowledge the following colleagues for their contributions to the discovery and characterization of the compounds disclosed in this manuscript. Heather Mcallister, Jiejun Wu, Sandrine Jolly, Laurence Queguiner, Sabastien Thomas, David Speybrouck, Judith Skaptason, Michael Hack, Kia Sepassi, Brian Scott, Joy Fuerst and Hector Novoa De Armas.

ABBREVIATIONS

CNS, central nervous system, IL-1β, interleukin-1β, DMPK, drug metabolism and pharmacokinetics, SAR, structure-activity relationship, CYP, cytochrome P450, MW, molecular weight, FLIPR, Fluorescence Imaging Plate Reader, p.o, per os, hERG, human Ether-à-go-go-Related Gene, PK, pharmacokinetics, MS mass spectrum, NHP, non-human primate, CL, clearance, V_{ss}, volume of distribution at steady state, $t_{1/2}$, half-life, %F, percent bioavailability, RLM, rat liver microsomes, HLM, human liver microsomes, MLM, mouse liver microsomes, CMLM, cynomolgus liver microsomes, PPB plasma protein binding, R.O., receptor occupancy, Bz-ATP, benzoyl adenosine triphosphate.

REFERENCES

1. Walker, E.; McGee, R. E.; Druss, B. G. Mortality in mental disorders and global disease burden implications: A systematic review and meta-analysis. *JAMA Psychiatry* **2015,** *72* (4), 334-341.

2. (a) Dowlati, Y.; Herrmann, N.; Swardfager, W.; Liu, H.; Sham, L.; Reim, E. K.; Lanctot, K. L. A Meta-analysis of cytokines in major depression. *Biol. Psychiatry* **2010,** *67* (5), 446-457; (b) Raison, C. L.; Capuron, L.; Miller, A. H. Cytokines sing the blues: inflammation and the pathogenesis of depression. *Trends Immunol.* **2006,** *27* (1), 24-31; (c) Bhattacharya, A.; Derecki, N. C.; Lovenberg, T.; C., D. W. Role of neuro-immunological factors in the pathophysiology of mood disorders. *Psychopharmacology* **2016,** *233* (9), 1623-1636.

3. (a) Goshen, I.; Kreisel, T.; Ben-Menachem-Zidon, O.; Licht, T.; Weidenfeld, J.; Ben-Hur, T.; Yirmiya, R. Brain interleukin-1 mediates chronic stress-induced depression in mice via adrenocortical activation and hippocampal neurogenesis suppression. *Mol. Psychiatry* **2008,** *13* (7), 717-728; (b) Koo, J. W.; Duman, R. S. Interleukin-1 receptor null mutant mice show decreased anxiety-like behavior and enhanced fear memory. *Neurosci. Lett.* **2009,** *456* (1), 39-

43; (c) Koo, J. W.; Russo, S. J.; Ferguson, D.; Nestler, E. J.; Duman, R. S. Nuclear factor-kappaB is a critical mediator of stress-impaired neurogenesis and depressive behavior. *Proc. Natl. Acad. Sci. U. S. A.* **2010,** *107* (6), 2669-2674; (d) Stokes, L.; Fuller, S. J.; Sluyter, R.; Skarratt, K. K.; Gu, B. J.; Wiley, J. S. Two haplotypes of the P2X7 receptor containing the Ala-348 to Thr polymorphism exhibit a gain-of-function effect and enhanced interleukin-1{beta} secretion. *FASEB J.* **2010,** *24* (8), 2916-2927.

4. Solle, M.; Labasi, J.; Perregaux, D. G.; Stam, E.; Petrushova, N.; Koller, B. H.; Griffiths, R. J.; Gabel, C. A. Altered cytokine production in mice lacking P2X(7) receptors. *J. Biol. Chem.* **2001,** *276* (1), 125-132.

5. Bhattacharya, A.; Biber, K. The microglial ATP-gated ion channel P2X7 as a CNS drug target. *Glia* **2016,** *64* (10), 1772-1787.

6. (a) Csolle, C.; Ando, R. D.; Kittel, A.; Goloncser, F.; Baranyi, M.; Soproni, K.; Zelena, D.; Haller, J.; Nemeth, T.; Mocsai, A.; Sperlagh, B. The absence of P2X7 receptors (P2rx7) on non-haematopoietic cells leads to selective alteration in mood-related behaviour with dysregulated gene expression and stress reactivity in mice. *Int. J. Neuropsychopharmacol.* **2013,** *16* (1), 213-233; (b) Iwata, M.; Ota, K. T.; Duman, R. S. The inflammasome: Pathways linking psychological stress, depression, and systemic illnesses. *Brain, Behav., Immun.* **2013,** *31*, 105-114.

7. (a) Iwata, M.; Ota, K. T.; Li, X. Y.; Sakaue, F.; Li, N.; Dutheil, S.; Banasr, M.; Duric, V.; Yamanashi, T.; Kaneko, K.; Rasmussen, K.; Glasebrook, A.; Koester, A.; Song, D.; Jones, K. A.; Zorn, S.; Smagin, G.; Duman, R. S. Psychological stress activates the inflammasome via release of adenosine triphosphate and stimulation of the purinergic type 2X7 receptor. *Biol. Psychiatry* **2016,** *80*, 12-22.

8. Keystone, E. C.; Wang, M. M.; Layton, M.; Hollis, S.; McInnes, I. B.; Team, D. C. S. Clinical evaluation of the efficacy of the P2X7 purinergic receptor antagonist AZD9056 on the signs and symptoms of rheumatoid arthritis in patients with active disease despite treatment with methotrexate or sulphasalazine. *Ann. Rheum. Dis.* **2012,** *71* (10), 1630-1635.

9. Eser, A.; Colombel, J. F.; Rutgeerts, P.; Vermeire, S.; Vogelsang, H.; Braddock, M.; Persson, T.; Reinisch, W. Safety and efficacy of an oral inhibitor of the purinergic receptor P2X7 in adult patients with moderately to severely active crohn's disease: A randomized placebo-controlled, double-blind, Phase IIa study. *Inflammatory Bowel Dis.* **2015,** *21* (10), 2247-2453.

10. Duplantier, A. J.; Dombroski, M. A.; Subramanyam, C.; Beaulieu, A. M.; Chang, S. P.; Gabel, C. A.; Jordan, C.; Kalgutkar, A. S.; Kraus, K. G.; Labasi, J. M.; Mussari, C.; Perregaux, D. G.; Shepard, R.; Taylor, T. J.; Trevena, K. A.; Whitney-Pickett, C.; Yoon, K. Optimization of the physicochemical and pharmacokinetic attributes in a 6-azauracil series of P2X7 receptor antagonists leading to the discovery of the clinical candidate CE-224,535. *Bioorg. Med. Chem. Lett.* **2011,** *21* (12), 3708-3711.

11. Stock, T. C.; Bloom, B. J.; Wei, N.; Ishaq, S.; Park, W.; Wang, X.; Gupta, P.; Mebus, C. A. Efficacy and safety of CE-224,535, an antagonist of P2X7 receptor, in treatment of patients with rheumatoid arthritis inadequately controlled by methotrexate. *J. Rheumatol.* **2012,** *39* (4), 720-727.

12. Ali, Z.; Laurijssens, B.; Ostenfeld, T.; McHugh, S.; Stylianou, A.; Scott-Stevens, P.; Hosking, L.; Dewit, O.; Richardson, J. C.; Chen, C. Pharmacokinetic and pharmacodynamic profiling of a P2X7 receptor allosteric modulator GSK1482160 in healthy human subjects. *Br. J. Clin. Pharmacol.* **2013,** *75* (1), 197-207.

13. Abdi, M. H.; Beswick, P. J.; Billinton, A.; Chambers, L. J.; Charlton, A.; Collins, S. D.; Collis, K. L.; Dean, D. K.; Fonfria, E.; Gleave, R. J.; Lejeune, C. L.; Livermore, D. G.; Medhurst, S. J.; Michel, A. D.; Moses, A. P.; Page, L.; Patel, S.; Roman, S. A.; Senger, S.; Slingsby, B.; Steadman, J. G.; Stevens, A. J.; Walter, D. S. Discovery and structure-activity relationships of a series of pyroglutamic acid amide antagonists of the P2X7 receptor. *Bioorg. Med. Chem. Lett.* **2010,** *20* (17), 5080-5084.

14. Letavic, M. A.; Lord, B.; Bischoff, F.; Hawryluk, N. A.; Pieters, S.; Rech, J. C.; Sales, Z.; Velter, A. I.; Ao, H.; Bonaventure, P.; Contreras, V.; Jiang, X.; Morton, K. L.; Scott, B.; Wang, Q.; Wickenden, A. D.; Carruthers, N. I.; Bhattacharya, A. Synthesis and pharmacological characterization of two novel, brain penetrating P2X7 antagonists. *ACS Med. Chem. Lett.* **2013,** *4* (4), 419-422.

15. Bhattacharya, A.; Wang, Q.; Ao, H.; Shoblock, J. R.; Lord, B.; Aluisio, L.; Fraser, I.; Nepomuceno, D.; Neff, R. A.; Welty, N.; Lovenberg, T. W.; Bonaventure, P.; Wickenden, A. D.; Letavic, M. A. Pharmacological characterization of a novel centrally permeable P2X7 receptor antagonist: JNJ-47965567. *Br. J. Pharmacol.* **2013,** *170* (3), 624-640.

16. Kovanyi, B.; Csolle, C.; Calovi, S.; Hanuska, A.; Kato, E.; Koles, L.; Bhattacharya, A.; Haller, J.; Sperlagh, B. The role of P2X7 receptors in a rodent PCP-induced schizophrenia model. *Sci. Rep.* **2016,** *6*, 36680.

17. Jimenez-Pacheco, A.; Diaz-Hernandez, M.; Arribas-Blazquez, M.; Sanz-Rodriguez, A.; Olivos-Ore, L. A.; Artalejo, A. R.; Alves, M.; Letavic, M.; Miras-Portugal, M. T.; Conroy, R. M.; Delanty, N.; Farrell, M. A.; O'Brien, D. F.; Bhattacharya, A.; Engel, T.; Henshall, D. C. Transient P2X7 receptor antagonism produces lasting reductions in spontaneous seizures and gliosis in experimental temporal lobe epilepsy. *J. Neurosci.* **2016,** *36* (22), 5920-5932.

18. Fischer, W.; Franke, H.; Krugel, U.; Muller, H.; Dinkel, K.; Lord, B.; Letavic, M. A.; Henshall, D. C.; Engel, T. Critical evaluation of P2X7 receptor antagonists in selected seizure models. *PLoS One* **2016,** *11* (6), e0156468.

19. Lord, B.; Aluisio, L.; Shoblock, J. R.; Neff, R. A.; Varlinskaya, E. I.; Ceusters, M.; Lovenberg, T. W.; Carruthers, N.; Bonaventure, P.; Letavic, M. A.; Deak, T.; Drinkenburg, W.; Bhattacharya, A. Pharmacology of a novel central nervous system-penetrant P2X7 antagonist JNJ-42253432. *J. Pharmacol. Exp. Ther.* **2014,** *351* (3), 628-641.

20. Dean, D. K.; Munoz-Muriedas, J.; Sime, M.; Steadman, J. G. A.; Thewlis, R. E. A.; Trani, G.; Walter, D. S. Preparation of Tetrahydro[1,2,4]triazolo[4,3-a]pyrazine Derivatives for Use as P2X7 Modulators. WO 2010125102 A1, November 4, 2010.

21. Rudolph, D. A.; Alcazar, J.; Ameriks, M. K.; Anton, A. B.; Ao, H.; Bonaventure, P.; Carruthers, N. I.; Chrovian, C. C.; De Angelis, M.; Lord, B.; Rech, J. C.; Wang, Q.; Bhattacharya, A.; Andres, J. I.; Letavic, M. A. Novel methyl substituted 1-(5,6-dihydro-[1,2,4]triazolo[4,3-a]pyrazin-7(8H)-yl)methanones are P2X7 antagonists. *Bioorg. Med. Chem. Lett.* **2015,** *25* (16), 3157-3163.

22. Savall, B. M.; Wu, D.; De Angelis, M.; Carruthers, N. I.; Ao, H.; Wang, Q.; Lord, B.; Bhattacharya, A.; Letavic, M. A. Synthesis, SAR, and pharmacological characterization of brain penetrant P2X7 receptor antagonists. *ACS Med. Chem. Lett.* **2015,** *6* (6), 671-676.

23. Swanson, D. M.; Savall, B. M.; Coe, K. J.; Schoetens, F.; Koudriakova, T.; Skaptason, J.; Wall, J.; Rech, J.; Deng, X.; De Angelis, M.; Everson, A.; Lord, B.; Wang, Q.; Ao, H.; Scott, B.; Sepassi, K.; Lovenberg, T. W.; Carruthers, N. I.; Bhattacharya, A.; Letavic, M. A. Identification of (R)-(2-Chloro-3-(trifluoromethyl)phenyl)(1-(5-fluoropyridin-2-yl)-4-methyl-6,7-di hydro-1H-

imidazo[4,5-c]pyridin-5(4H)-yl)methanone (JNJ 54166060), a small molecule antagonist of the P2X7 receptor. *J. Med. Chem.* **2016,** *59* (18), 8535-8548.

24. Ameriks, M. K.; Ao, H.; Carruthers, N. I.; Lord, B.; Ravula, S.; Rech, J. C.; Savall, B. M.; Wall, J. L.; Wang, Q.; Bhattacharya, A.; Letavic, M. A. Preclinical characterization of substituted 6,7-dihydro-[1,2,4]triazolo[4,3-a]pyrazin-8(5H)-one P2X7 receptor antagonists. *Bioorg. Med. Chem. Lett.* **2016,** *26* (2), 257-261.

25. (a) Ziff, J.; Rudolph, D. A.; Stenne, B.; Koudriakova, T.; Lord, B.; Bonaventure, P.; Lovenberg, T. W.; Carruthers, N. I.; Bhattacharya, A.; Letavic, M. A.; Shireman, B. T. Substituted 5,6-(Dihydropyrido[3,4-d]pyrimidin-7(8H)-yl)-methanones as P2X7 antagonists. *ACS Chem. Neurosci.* **2016,** *7* (4), 498-504; (b) Chrovian, C. C.; Soyode-Johnson, A.; Ao, H.; Bacani, G. M.; Carruthers, N. I.; Lord, B.; Nguyen, L.; Rech, J. C.; Wang, Q.; Bhattacharya, A.; Letavic, M. A. Novel phenyl-substituted 5,6-Dihydro-[1,2,4]triazolo[4,3-a]pyrazine P2X7 antagonists with robust target engagement in rat brain. *ACS Chem. Neurosci.* **2016,** *7* (4), 490-497.

26. Lord, B.; Ameriks, M. K.; Wang, Q.; Fourgeaud, L.; Vliegen, M.; Verluyten, W.; Haspeslagh, P.; Carruthers, N. I.; Lovenberg, T. W.; Bonaventure, P.; Letavic, M. A.; Bhattacharya, A. A novel radioligand for the ATP-gated ion channel P2X7: [3H] JNJ-54232334. *Eur. J. Pharmacol.* **2015,** *765*, 551-559.

27. (a) Altman, R. A.; Koval, E. D.; Buchwald, S. L. Copper-catalyzed N-arylation of imidazoles and benzimidazoles. *J. Org. Chem.* **2007,** *72* (16), 6190-6199; (b) Antilla, J. C.; Baskin, J. M.; Barder, T. E.; Buchwald, S. L. Copper−diamine-catalyzed N-arylation of pyrroles, pyrazoles, indazoles, imidazoles, and triazoles. *J. Org. Chem.* **2004,** *69* (17), 5578-5587.

28. Khanna, I. K.; Weier, R. M. Regiospecific addition of Grignard reagents to the 4-position of activated imidazo[4,5-c]pyridine. A convenient method fot the synthesisof 4-alkylarylimidazopyrazines. *Tett. Lett.* **1993,** *34* (12), 1885-1888.

29. Deng, X. H.; Liang, J.; Allison, B. B.; Dvorak, C.; McAllister, H.; Savall, B. M.; Mani, N. S. Allyl-assisted, Cu(I)-catalyzed azide-alkyne cycloaddition/allylation reaction: Assembly of the [1,2,3]triazolo-4,5,6,7-tetrahydropyridine core structure. *J. Org. Chem.* **2015,** *80* (21), 11003-11012.

30. Alcazar Vaca, M. J., Andres Gil, J. I., Chrovian, C. C., Coate, H. R., De Angelis, M., Gelin, C. F., Letavic, M. A., Savall, B. M., Soyode-Johnson, A., Stenne, B. M., Swanson, D. M. Preparation of Imidazo[4,5-c]pyridines and 1,2,3-Triazolopyridines as P2X7 Modulators for Therapy. US 2014 0275015 A1 September 18, 2014.

Table of Contents Graphic

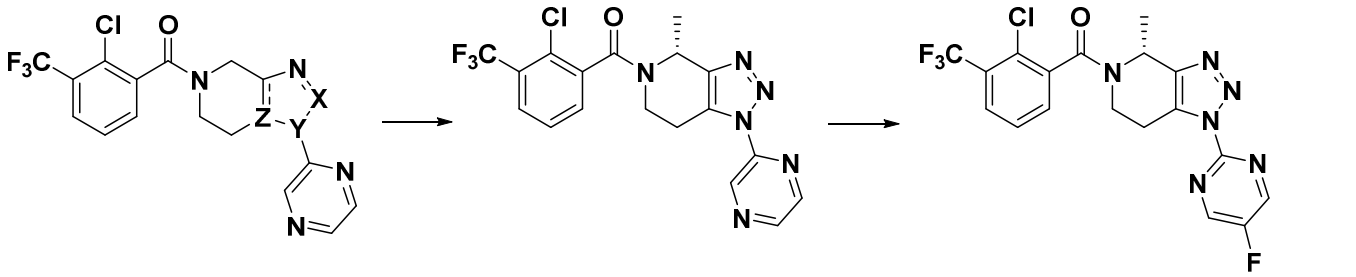

Prototype Lead Series
X, Y, Z= C or N

11
Optimized lead
Improved potency
Human dose prediction 300 mg b.i.d.

14
Optimized clinical candidate
SIgnificantly improved PK profile
Human dose prediction, 8 mg q.d.